2015

Design and Development of a Ventilation Chamber for Testing Efficacy of Tracheal Stents

Caroline N. Horton
University of South Carolina

Design and Development of a Ventilation Chamber for
Testing Efficacy of Tracheal Stents

By

Caroline N. Horton

Bachelor of Science
University of South Carolina, 2013

Submitted in Partial Fulfillment of the Requirements

For the Degree of Master of Science in

Biomedical Engineering

College of Engineering and Computing

University of South Carolina

2015

Accepted by:

David N. Rocheleau, Director of Thesis

M. Damon Kolok, Reader

Lacy Ford, Senior Vice Provost and Dean of Graduate Studies

Acknowledgements

I would like to first thank Dr. David Rocheleau for his continued guidance and patience with me as I struggled to design a chamber worthy of this degree. I know that there were many times I felt like giving up, but Dr. Rocheleau found a way for me to push forward.

In addition, I would like to thank Dr.'s Franklin McGuire, Damon Kolok, and Maria Del Mar Cirino, for providing their expertise and guidance as related to the field of pulmonology. This work was developed due to a need that they felt should be addressed, and without their insight, this project would have never begun.

I am very grateful for the help I've received from Mike Gore and Burt Ward in the School of Medicine and Mechanical Engineering Machine Shops, as both were incredibly helpful in converting my rough sketches to viable chamber options, and provided valuable input for the best design.

Also, the efforts of my fellow researchers on this project, Zach Schwab and Nidah Hussain, have not gone unnoticed. Zach's help in particular was instrumental in testing of the designs, as I often used him as the muscle behind the pumps. I am also very grateful to my friends and family for putting up with me and even providing advice. Specifically, my parents, Clyde and Susan, and friends, Adam, Rebecca, Brook, and Courtney.

Abstract

Tracheobronchial malacia results in a weakening of the tracheal walls, leading to increased difficulty breathing. Stents are used to reopen the lumen of the trachea, however, current models are not personalized to each patient, leading to migration, inflammation, and breakage of the stents. In order to successfully test novel stent designs, a ventilation chamber is needed to recreate the breathing conditions of the body.

The following describes the iterative development of a ventilation chamber, which allows inflation and deflation of lungs via negative pressure ventilation, as representative of an actual body undergoing respiration. Previous work shows that lungs are not generally used as the testing medium, as only excised portions of trachea are used. The chamber presented here would allow testing to the primary and secondary bronchi, which is beneficial to medical practitioners. This chamber would be utilized for simulating an *in vivo* environment, in which, tracheal and bronchial stents may be tested and analyzed. The chamber described is of simple, replicative design, with attachment of a bladder acting as a diaphragm, which is expanded and reduced to recreate representative pressures of the chest cavity. A trachea and lungs, porcine in nature for testing purposes, are attached at the opposite end of the chamber, via a conduit allowing them to remain open to atmosphere, allowing the lungs to inflate via negative pressure.

An appropriately sized chamber was developed, as well as estimation of appropriate applied pressure to achieve ventilation.

Table of Contents

List of Figures

List of Tables

Chapter 1: Literature Review of Existing Pulmonary Stent Designs, Inflammatory Response, and Current Chamber Designs

As rapidly as healthcare evolves, one aspect, pulmonary stent design and administration, remains fairly rudimentary. Pulmonary (airway) stents have been in use for approximately 100 years, yet among the numerous types of stents which have been developed in the subsequent years, the efficacy of placement continues to prove complicated (Chin et al. 2008). Bioactive and bioabsorbable stents which integrate and improve the tracheal tissue are yet to be perfected. The following provides a discussion of the existing stent designs, as well as an introduction to animal testing methods, ex vivo lung chambers for preliminary testing, and using computerized tomography to aid in the personalization of stents.

1.1 Existing Pulmonary Stents

Pulmonary (or airway) stents are hollow tubular prostheses, which allow for air passage through the lumen in the event of a weak or damaged bronchial tree. These stents are often used to re-establish lumens by holding them open; this can be due to bronchomalacia, which is a weakening or collapse of the cartilage supporting the trachea; in response to tumor in-growth; or as a treatment against fistulas (abnormal connection between tissue) and dehiscences (rupture of a previously closed wound) to the esophagus or pleural cavity (Chin et al. 2008; Freitag 2000). In order to provide the best results for the patient, type, width, and length must be thoroughly examined and selected, as there are

a multitude of possible stent choices, which can be grouped to include silicone or balloon dilated, covered, and self-expanding metal stents (Chin et al. 2008; Freitag 2000).

Silicone stents, such as Dumon, Hood, and Polyflex, are disadvantageous in many situations as they do not allow for cilia penetration, and are often slightly loose in the trachea, causing migration and discomfort for the patient. However, silicone stents do resist compression and are more easily removed than their metal counterparts, although realignment can be difficult (Chin et al. 2008). Metal stents, such as Strecker and Palmaz in the balloon dilated category, Ultraflex and Gianturco Z in the self-expanding category, and Wallstent and Alveolus as covered self-expanding examples, are prone to fracture, as external pressure wears them down over time, and they also have the potential to cause necrosis of the mucosa, and fistula formation, making them difficult to remove (Chin et al. 2008). The beneficial aspects of metal stents include their thinner frame, which allows for more clearance through the lumen; they experience less migration; have less interference with cilia; and in the case of covered metal stents, can block tumor growth along the length of the stent (Chin et al. 2008).

It is important for mucus clearance to occur, which is generally at a rate of less than 5 mL a day; however, in the event of inflammation and/or irritation, excessive secretions considered sputum, become problematic and must be cleared by coughing, which can lead to even more irritation within the airway (Freitag 2000). Another downfall of the majority of stents produced is that they are mostly circular, which does not directly correlate to the anatomy of the trachea, as it could be described as more “D” shaped, as it is semicircular, with a flat side that lies against the esophagus. Figure 1.1 provides a visual overview of the vast array of available airway stents.

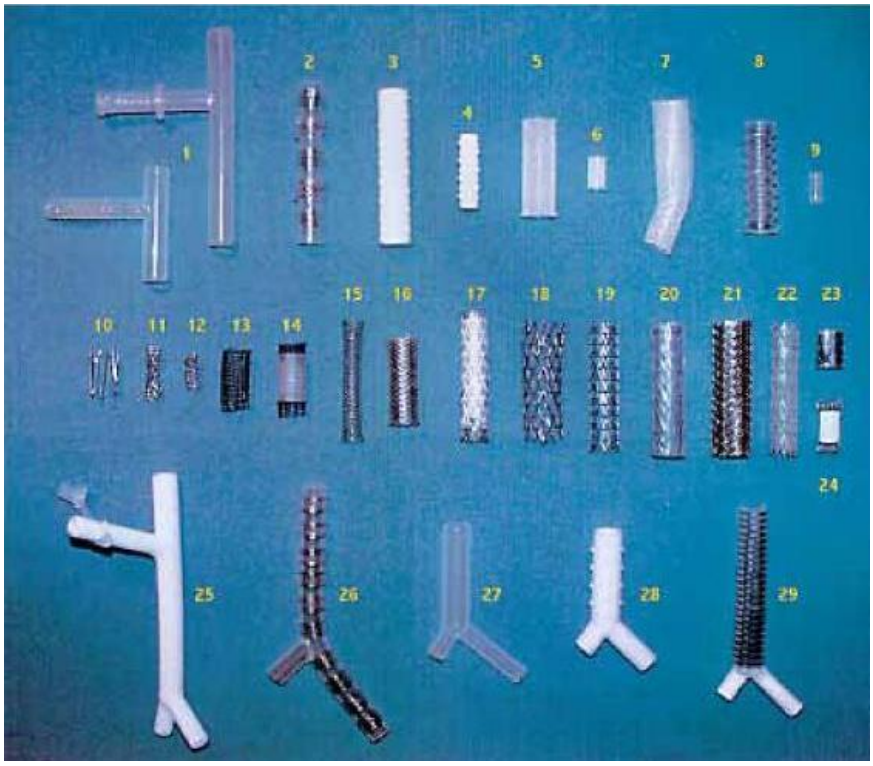

1. Montgomery T-tubes
2. Orlowski tracheal stent
3. Dumon tracheal stent
4. Dumon bronchial stent
5. Polyflex tracheal stent
6. Polyflex bronchial stent
7. Polyflex stump stent
8. Noppen tracheal stent
9. Hood bronchial stent
10. Gianturco stent
11. Palmaz stent
12. Tantalum Strecker stent
13. Uncovered Ultraflex stent
14. Covered Ultraflex stent
15. Uncovered Wallstent
16. Covered Wallstent
17-24. Prototypes of metal stents and compound stents currently tested preclinically and clinically
25. Westaby stent
26. Bifurcated Orlowski stent
27. Hood Y-stent
28. Bifurcated Dumon stent
29. Dynamic stent

Figure 1.1. Overview of currently available stents (Freitag 2000). The Dynamic stent is listed as piece 29, also, the Dumon (3-4, 28), Polyflex (5-7), Hood (9), Gianturco (10), and Palmaz (11) which were some of those previously mentioned.

The Freitag dynamic stent is the only current "D" shaped airway stent on the market, which was developed through analysis of CT-scans of various patients. This stent consists of steel horseshoe shaped struts enveloped in silicone, with a silicone face without struts that makes up the flat side that lies against the esophagus. These steel struts are useful in maintaining the lumen against external compression, whereas the silicone face without struts allows for compression during cough (Freitag et al. 1994). The struts are also spaced at intervals similar to those of the cartilaginous rings surrounding the trachea, which helps to prevent migration, as the struts should fit snugly between the rings. In addition, the length can also be cut to fit more appropriately to each patient (Freitag et al. 1994). This design can be observed more closely in Figure 1.2, which also shows the slight increase in diameter towards the bifurcation point.

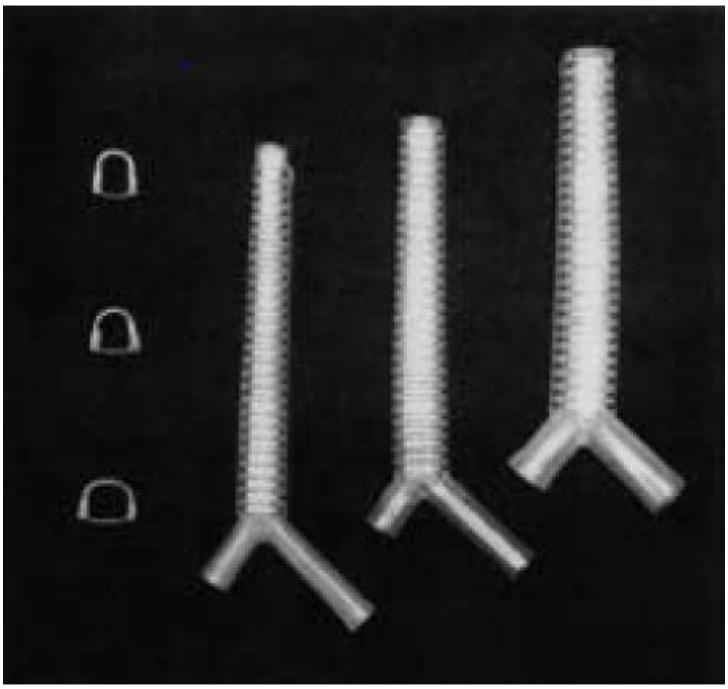

Figure 1.2. Examples of Freitag stent, in three different sizes (Freitag et al. 1994). To the left is a representation of the increase in size towards the bifurcation point. The steel struts can be seen, which are horseshoe shaped, and do not interfere with the solid silicone back wall.

Freitag et al., described the importance of a dynamic stent after analyzing CT-scans of tracheas, and finding that they are not uniformly structured throughout (Freitag et al. 1994). As such, they were also able to model the effects of normal airway breathing and coughing when stents of different types were in place. Unlike the Freitag stent, most stents do not allow for a cross-sectional change in lumen diameter during coughing and forced exhalation, the critical velocity of airflow to move mucus is not reached; this can cause mucus buildup and blockage, which can be just as problematic as a weak walled trachea. Freitag et al. approximates that fifteen percent of patients with airway stents develop clinically significant obstruction due to inspissated secretions, since the cilia, which would typically help push mucus and sputum upwards, are blocked (Freitag et al. 1994). This led to their design that incorporates the flat membrane to allow for dynamic motion in the trachea through reduction of cross-sectional area, which would help sputum clearance.

Unfortunately, this stent is often skipped by medical professionals at times as it is difficult to deploy and remove, even though it is most similar to natural trachea shape.

Preliminary data produced by Freitag et al. describes the changes in diameter that the trachea undergoes when rigid and dynamic stents are present, and their ability to respond to coughing, to show that a "D" shaped stent would be most effective. The results of coughing can be seen in Figure 1.3, which illustrates the velocity of air through the lumen, which is lowest in the rigid stent model. In addition, these tests showed that an ideal stent should be able to change in regard to cough pressures; this is accomplished by the flexible membrane on the posterior side of the stent, which allows for reversible reduction of cross-sectional area. The use of a silicone flexible membrane also counteracts the tendency of metal stents to induce disproportionate granulation formation when exerting high localized pressures (Freitag et al. 1994).

In the design of the Freitag stent, one hundred and fifty patients' airways were modeled using computed tomography (CT) to determine shape profiles which include the average and standard deviation for the regions one centimeter below the vocal cords, the middle of the trachea, and one centimeter above the carina, and is presented in Figure 1.3 as well (Freitag et al. 1994). This image also shows how the models depict the flattening of the trachea as one progresses up cephalically from the carina towards the cricoid. By reproducing this information through computer-aided design (CAD) software, models were made that determined the average branching angles at the carina from the main bronchus to be 144.7±4° to the right and 133.3±3° to the left, depicted in Figure 1.4 (Freitag et al. 1994).

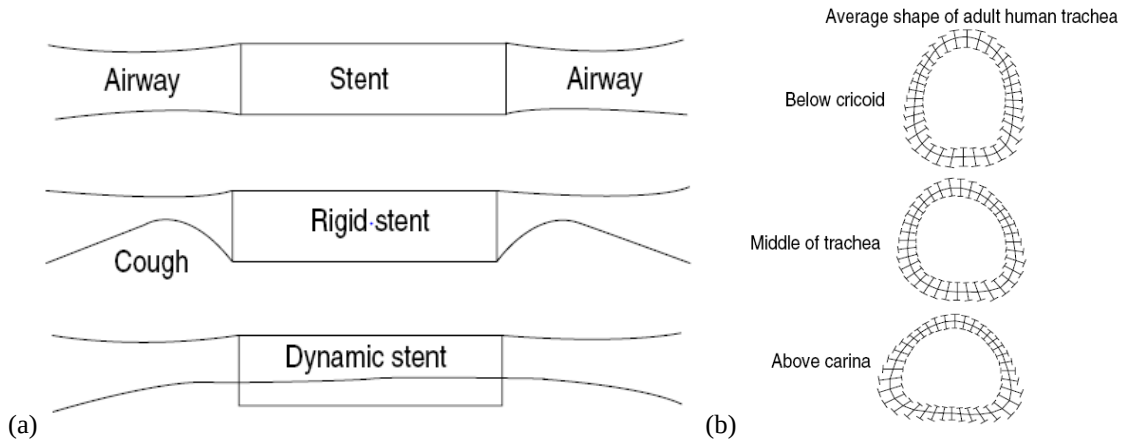

Figure 1.3. Shape profile of trachea. (a) Depiction of tracheal diameter change subjected to rigid and dynamic stents. When flow is equal through the lumen, the velocity in the rigid stent is the lowest (Freitag et al. 1994). (b) Average shape of trachea determined through CT-scans of 150 patients (Freitag et al. 1994). Bars indicate variance of the standard deviation at each point.

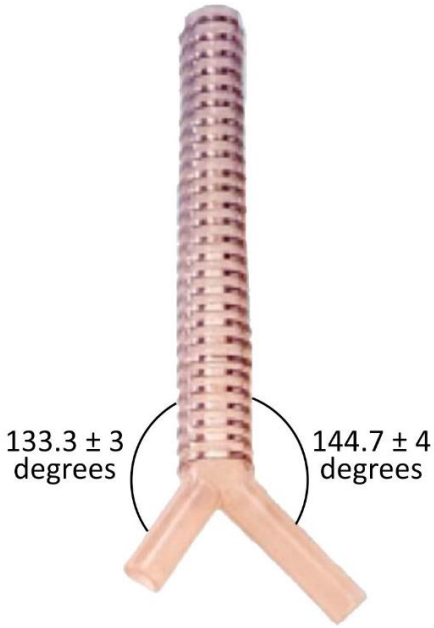

Figure 1.4. Branching angles at the carina from the main bronchus.

1.2 Animal Testing

Piglets and adult mini-pigs that weigh 23 ± 6 kilograms on average, have been found to have tracheas of similar size to humans between 45 and 60 kilograms (99 - 132 pounds), making them a good representative model for stent testing, as the same size

instruments can be used for both species (Marquette et al. 1995). As such, Marquette et al. describe in detail methods for inducing malacia in pigs, which is improved upon by Saueressig et al. After induction of malacia and stent deployment, inflammatory response can be analyzed through tests such as reverse-transcriptase polymerase chain reaction (RT-PCR) and enzyme linked immunosorbent assays (ELISA).

Before inducing malacia, the animals must be placed under general anesthesia, after 8 hours of fasting from food and water (Saueressig et al. 2011), and in the case of Marquette et al., intravenous propofol was used at 2 to 3 mg/kg to begin, with a continuous infusion at 10 mg/kg·hr (Marquette et al. 1995). Ventilation was also provided during surgery either by a cannula at the proximal port of endotracheal tube, or to the rigid bronchoscope. To create the malacia, extramucosal resection of approximately 50% of the circumference of three consecutive cartilaginous arches is performed, then, beginning two weeks later, a 23% solution of NaOH at pH 14 was applied to the mucosal area (inside the trachea) at the level of the resected cartilaginous arches via cotton swab (Marquette et al. 1995). As determined by Marquette et al., and confirmed by Saueressig et al., the best technique for NaOH application is to restrict the application to two thirds of the bronchial circumference, or avoid the posterior wall, because the caustic properties of the solution will become too severe if the entire circumference is treated (Marquette et al. 1995; Saueressig et al. 2011). Subsequent application of the solution was carried out during weekly bronchoscopies, as needed, to remove necrotic tissue after stenosis of greater than 50% was found, although three applications was typical (Marquette et al. 1995; Saueressig et al. 2011).

Stent deployment of an uncovered Palmaz stent into these porcine tracheas induced granulation formation which reached its peak after the 7th day, and resolved itself by day

21; however, after day 21, the stent was no longer molded to the bronchial wall due to moderate to severe crushing of greater than 50% (Marquette et al. 1995). Dacron covered Palmaz stents migrated distally, and thus blocked the left upper lobe bronchus, resulting in pneumonia; and two tests with covered self-expanding stents were deemed inconclusive overall as one stent was expectorated, and in the other case, the pig died due to respiratory obstruction 4 days after the operation, though it was determined the stent did migrate proximally during that short amount of time (Marquette et al. 1995).

Fibrosis and necrosis were found to occur in the region of the excised cartilaginous arches, mainly in the submucosal and adventitious layers (Saueressig et al. 2011). In order to determine the latero-lateral and anteroposterior diameters of the tracheal lumen, the program Sigmascan Demo-Image Analyser by Sigma, was utilized, which uses the equation:

$$Area\ (mm^2) = \pi \cdot \frac{sagittal\ diameter\ (mm)}{2} \cdot \frac{coronal\ diameter\ (mm)}{2} \qquad eq.1$$

to calculate the area of the tracheal lumen (Saueressig et al. 2011). Tracheal inflammatory stenosis (narrowing) and malacia are caused by trauma and ischemia, a restriction of blood supply, to the mucosa, therefore calculating the area proves valuable to quantify the presence of inflammation and fibrosis (Saueressig et al. 2011).

It is most typical for granulation tissue to form as a result of impaired mucosal blood supply (Freitag et al. 1994); therefore, with regard to inflammatory response in live models, testing of an array of cytokines can be performed to quantify immune response. The body houses a multitude of cytokines, which is a broad term that describes factors that regulate cell activity, and if they become too numerous, tissue damage or death can occur (Costa et al. 2013); these can range from interleukins (IL), to tumor necrosis factors (TNF),

or transforming growth factors (TGF), and interferons (IFN), etc. As each regulating factor has different activity and targets, these can be used to develop an overall understanding of the immune response to a particular "intruder" through assays such as the previously mentioned RT-PCR and ELISA.

These processes are different in that ELISA utilizes antibody specificity to test for the presence of an antigen in the sample, which is generally displayed through a color change, whereas RT-PCR is a process that allows for the formation and amplification of complementary DNA strands, which are analyzed for gene expression through the quantification of fluorescent probes linked to the cDNA (Thanawongnuwech et al. 2004). This quantification has taken the place of northern blotting, which was previously the standard used to separate RNA based on applying a charge to an agarose gel stained with an UV fluorescent material such as ethidium bromide, the gel acts to trap the molecules based on their size and structure (Thanawongnuwech et al. 2004).

Previously, Dozois et al., provided the basis for targeting and evaluating porcine cytokine expression through the determination of the oligonucleotide sequences necessary for gene specificity through RT-PCR. In addition, Dozois et al. was able to determine the optimal range of PCR amplification cycles to be between 27 and 38, as well as detect the presence of two housekeeping genes that are useful during RT-PCR, β-actin and cyclophilin (Dozois et al. 1997). However, one of the most important things to remember about RT-PCR is that it does not allow for comparison of the amount of mRNA between cytokines, as the quantitative amounts are in relation to the whole (Dozois et al. 1997). Also, protein levels must be separately tested as mRNA levels are not necessarily reflective

of the amount of protein being produced (Dozois et al. 1997). Both tests are useful as they can be completed fairly quickly, and only small amounts of starting material is needed.

During testing of the live animal models, bronchoalveolar lavage (BAL) can be used to collect epithelial lining fluid and bronchoalveolar cells, after flushing the cells with phosphate buffered saline (PBS) (Costa et al. 2013). This fluid may then be tested for cytokines such as IL-1α, IL-1β, IL-2, IL-4 Il-6, IL-8, IL-10, IL-12, TNF-α, TGF-β1, and IFN-γ which are all classified as proinflammatory cytokines, which essentially means an increase in their production leads to an increase in inflammatory response (Thanawongnuwech et al. 2004). TNF-α and TGF-β1 are considered integral in the formation of granulation tissue and fibrosis accumulation as the former acts as a trigger for fibrosis occurrence, and the latter is a direct growth factor for fibroblast proliferation and extracellular matrix production (Xing et al. 1997). In pigs infected with *Mycoplasma hyopneumoniae*, the levels of IL-1, Il-6, and TNF-α are seen to increase; however, in pigs infected with swine influenza, IL-1 and TNF-α levels are decreased (Thanawongnuwech et al. 2004). This shows the variability of response, which is why blanket testing of numerous cytokines is important, as thus far, the cytokine responses in pigs is not as well outlined as in humans.

In the experiments performed by Thanawongnuwech et al., levels of cytokine response and the correlating protein production were evaluated at 10, 28, and 42 days after initial infection with *M. hyopneumoniae* to determine if specific cytokines could be associated with certain acts (Thanawongnuwech et al. 2004). It was determined that although many of the cytokines expressed increased levels, IL-10 was most likely responsible for ongoing persistence of the infection, as it is an inhibitor of macrophage

function (Thanawongnuwech et al. 2004). As the concentration was dramatically increased, it is thought that it was able to alter the targets of the host immune response away from a Th1-type response, which should have cleared the infection (Thanawongnuwech et al. 2004). In addition, IL-12 levels remained high over the course of the 42 days, leading to increased production of interferon-γ, which when over-produced may lead to autoimmune disorders. RT-PCR was used with all of the previously listed cytokines to determine density, and ELISA assay was used to measure the levels of IL-1β, IL-8, IL-10, and TNF-α at undiluted concentrations (Thanawongnuwech et al. 2004).

1.3 Existing Lung Chambers

Prior to animal testing, it is important to determine the viability of stent design through the use of excised lungs in a chamber that replicates breathing, so as to reduce the probability of injury to a live animal. As porcine lungs are relatively easy to acquire, one does not need to be euthanized for the sole purpose of performing viability tests.

Freitag et al. placed excised tracheas in a Plexiglas chamber with the distal ends of the trachea attached to a 10 L tank, which acted as a lung proxy, in order to study the behavior of deployed stents during forced expiration, cough, and extrinsic compression. Negative and positive pressures were applied to the chamber via a vacuum and pressure source which alternated between +5 and -9 kPa (0.725 to -1.305 psi). In these experiments, a cough was replicated through the attachment of a computer-controlled vibration device, which produced quick pressure swings between +3 and -9 kPa (0.435 to -1.305 psi) (Freitag et al. 1994). A comparison between the natural tracheal peak flow velocity to the peak flow velocity with a rigid stent in place illustrates the importance of a dynamic stent design in that the rigid stent only allowed for approximately half of the natural maximum velocity

with values of 87 m/s and 50 m/s, respectively (Freitag et al. 1994). Testing of compliance also demonstrated that even with large variations of natural tracheas (opposite effects of patient with emphysema vs. patient with heart failure and no pulmonary disease), deployment of a dynamic stent led to similar mechanical behavior between the cases when comparing cross-sectional area to pleural pressure (Freitag et al. 1994).

Research conducted by Lilburn et al., used rodents to investigate airway responses by performing *ex vivo* negative pressure lung ventilation, which included a right ventricle catheter insertion to allow for flushing of the remaining pulmonary blood after excision with heparin-saline solution and Dublecco's PBS (Lilburn et al. 2013). The heart and lungs were then moved together into an acrylic ventilation chamber with the trachea pointed downwards and suspended in 5% w/v glucose solution, which helped to curtail dehydration and edema of the tissues (Lilburn et al. 2013). The researchers used the suction properties of negative pressure ventilation to fill the lungs with air, then released the pressure to allow for exhalation. A water bell was used to determine the volume of exhaled air by measuring the volume of displaced water (Lilburn et al. 2013).

Patents filed by Burt B Orden (US 4,167,070 A) and Robert H Estetter, et al. (US 6,874,501 B1) both describe techniques of chamber construction using rigid, translucent materials, to create the overall housing, which describe chambers similar to the goal of the present research (both depicted in Appendix A). The patent filed by Orden, was published in 1979 and consisted of three air filled chambers, two of which housed single bladder flexible membranes to represent lungs, which could be in communication with each other by a conduit, while also isolating the air flow from the chambers to the interior of the lung simulating structures on each side (Orden 1979). In this design, two sets of bellows are

present. One set is used to replicate the pressures caused by the muscles within the chest when the arms are lifted and lowered; whereas the other represents the diaphragm. Both sets of bellows work in similar manners, by increasing the pressure surrounding the lungs when the corresponding bellows is collapsed, and decreasing the pressure when the bellows are expanded, which provides the negative pressure needed for inspiration (Orden 1979). For this schematic, the chambers are filled with air around the lungs, and each bellow works independently of the others. To alter the pressure within the flexible simulated lung, a pump, such as an alternating piston pump in this rendering, is used. Mass elements are added to ensure that the position of the housing does not affect the simulated lung; these work by applying pressure to the lung(s) to recreate various lung conditions for illustration in erect, supine, and prone positions (Orden 1979).

US patent number 6,874,501 B1, filed by Robert H Estetter et al. in 2002, looked to improve upon the existing design proposed by Orden by introducing liquid around the lungs, as well as modifying the design to better represent lungs in the human body. As liquid is known to normally surround the lungs, this change enables a more realistic simulation. In addition, Estetter et al., described that Orden's mass elements were not symmetrically placed, his simulated lungs only consisted of single bladders surrounded by air, that his terminology was backwards to his depiction, and that these discrepancies would lead to results that do not accurately replicate the activity of the lungs (Estetter et al. 2005). In order to address these disparities, Estetter et al. first increased the amount of lung bladders to match the amount of lobes a human has, of three on the right, and two bladders/lobes on the left side. Each bladder is connected to a valve, which allows for not only both sides to work independently, but also each bladder. In addition, a rigid plate was

mounted to be fluid tight between the left and right lungs, to represent the mediastinum, which is described as the area between the lungs, normally filled by the heart, trachea, bronchi, and esophagus. As the simulator houses materials meant to act as replicas of the organs, to simulate their separation, this plate was added, to further the ability of each side to act independently of the other. It is the opinion of Estetter et al. that the use of fluid surrounding the lungs is a better method than rigid mass elements on the lung surface to simulate gravitational effects of chamber rotation, so they chose to dismiss this aspect of design from Orden's chamber (Estetter et al. 2005).

Both designs choose to include a bladder in representation of the heart as well; however, both place the heart at opposite ends of their design from the trachea, which does not correlate with anatomical correctness. Orden and Estetter et al. both describe the inclusion of the heart bladder as a way to show how hyperinflation, as a representation of an enlarged heart, will affect lung compliance. Orden accomplishes this by having the flexible bladder representing the heart adjacent to a flexible portion of the otherwise rigid wall separating the heart and lung cavities (Orden 1979). The heart and flexible portion of wall are on the opposite end of the chamber from the simulated trachea, and therefore not nestled in the lung, as in an actual person, it is unclear if this affects the outcome of simulations to a high enough degree to be problematic. Estetter et al. also use a flexible bladder to show how an enlarged heart can affect the lungs, but surprisingly do not place theirs next to the left lobes of the lungs either, although it is again unclear if this is an issue. Estetter et al. attach their heart bladder to the opposite end of the mediastinum, away from the simulated trachea, in a placement that allows the diaphragm to be displaced upon

inflation, thereby affecting the effect of the diaphragm on the cavity and lung (Estetter et al. 2005).

1.4 Stent Customization

Ongoing research in the development of new stents mainly includes the availability of customization, but there are also prototypes of nitinol stents that are temperature dependent with the ability to be adjusted in vivo, as well as the possibility of inclusion of phosphorus-32 , which would prevent the development of granulation tissue (Freitag et al. 1994; Tripuraneni et al. 2012). One case of customization came out of desperation for a patient of low socioeconomic standing, who could not afford a prefabricated device. Therefore, it was determined cost-effective to develop a heat polymerized acrylic stent, as biocompatibility was already proven (Tripuraneni et al. 2012). Polyether was used as an impression material, with an incorporated stainless steel wire to stabilize the mold (Tripuraneni et al. 2012). Another approach to the custom route is being taken by Melgoza et al., as they develop a program that integrates CAD to build custom stents.

The use of CAD allows the researchers to utilize the theory of inventive problem solving with the process of quality function deployment which helps solve physical contradictions related to geometry and material, to develop designs that will decrease the product development cycle and costs, and increase the quality of individual designs (Melgoza et al. 2012). The product design has the goals of “necessities” which include biocompatibility, where no cytotoxicity is displayed by the prostheses; low migration rate, with hopes of avoiding greater than 4 mm of vertical displacement; easy insertion and removal, which is obtained by striving to match an elastic modulus between 1 and 15 MPa; and lastly, the dynamic property which will come from a reduced wall thickness (Melgoza

et al. 2012). CT-scans were used to configure stent design with the manufacturing device "Fab@Home" which can translate files of stereolithography format into three-dimensional silicone product. The final design does contain a flat posterior portion, with a diameter of 1 mm, with a wavy vertical pattern (diameter = 2 mm) that is meant to fit between the cartilaginous rings, spaced 10 mm apart (Melgoza et al. 2012). The future of this work requires streamlining the printing process, as well as developing ways to ensure sterility and most importantly, viability in the patient.

Through the stepwise process of developing a feasible design, which succeeds in isolated tests through the pressure chamber, and then the live model, the desired result is a biocompatible model that does not induce great inflammatory response. Due to the existing knowledge of porcine cytokinetic responses, the applicable assays will help to validate success.

Chapter 2: Design Development

An appropriate ventilation chamber to house actual lungs is necessary for recreating the conditions of the chest cavity, as a method to test novel stents, which have the goal of being designed uniquely for individual malacias. To replicate conditions within the chest cavity, an ideal chamber should be able to undergo negative pressure, as the lungs rely on negative pressure ventilation for respiration.

Normal respiration occurs through the involuntary muscle control of the diaphragm lifting and lowering at the bottom of the rib cage, as the rib cage expands and contracts. The physiological action of inhalation is described by Grotberg (2009) as air being pulled into the lungs through a vacuum created by the diaphragm contracting downward, also pulling the lungs downward, in conjunction with the contraction of the external intercostal muscles lifting the lower six ribs; this vacuum causes negative pressure in the lungs. Exhalation acts in the reverse manner, reversing the vacuum as the diaphragm and external intercostal muscles relax, allowing air to leave the lungs (Grotberg 2009).

Negative pressure ventilation also allows for regular hyperinflations to occur, to overcome decreasing lung compliance due to decreasing surfactant levels during normal respiration (Uhlig & Wollin 1994). During hyperinflation, which occurs in the body approximately every five minutes as a deep breath, surfactant levels are regenerated, which helps the alveoli remain open as they overcome a lower surface tension with the help of surfactant, therefore avoiding atelectasis, a complete or partial collapse of the lung (Uhlig & Wollin 1994).

Some testing methods, such as those stated by Freitag et al. (1994) do implement the use of actual human tracheal tissue, although, only a section of a single trachea was obtained from the donor to measure how well a variety of stents hold open the lumen, with a tank attached at one end to act as a lung. In this case, stents are deployed and removed from the same sample successively, which is not ideal for later deployments which are subjected to progressively worsening conditions, as deterioration occurs inside the lumen. Since Freitag et al. only used a section of trachea, this was not ideal for the purposes of the Tracheobronchial Stent Design (TSD) team due to the desire to target the primary, and potentially, secondary bronchial region of the lungs. In addition, this methodology was not repeated here because of the use of positive pressure ventilation, which occurs when air is forced into the lungs, and is not ideal for testing with lungs as this sort of ventilation can lead to over-inflation and edema formation, causing damage to the lung (Uhlig & Wollin 1994). Most simulation devices on the market use plastic and silicone lungs or sacs, and even more rely on positive pressure ventilation, therefore, a new chamber needed to be designed.

Because negative pressure ventilation is preferred, it was the goal of this research to design a chamber that would meet the aforementioned conditions of housing lungs and performing ventilation by negative pressure. If successful, the chamber would provide a method to test novel stents beyond the main tracheal region to the primary and secondary bronchi of the respiratory tree. Therefore, there is a need for the use of actual lungs, and porcine lungs were chosen due to their similarity in size and ease of access to obtain. By performing tests with porcine lungs, measurements are more accurate and realistic than those performed with synthetic materials. The following schematic depicts the needs of the

system, which includes the chamber itself; a way to monitor pressure changes; a conduit to attach the trachea to the chamber, allowing it to be open to atmosphere; lungs; diaphragm; and control mechanism of diaphragm to adjust pressure similarly to the mechanism used in the body.

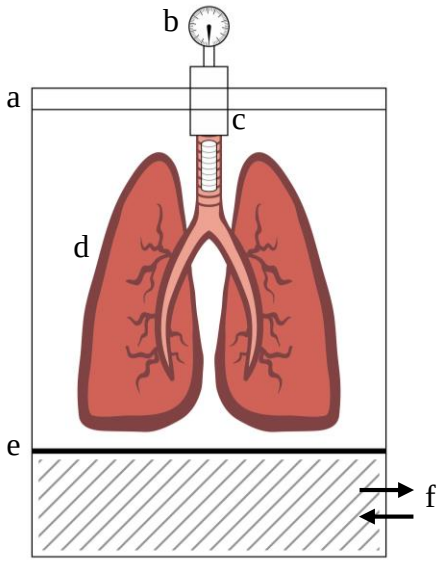

Figure 2.1. Schematic of design constraints. Proposed design needs to house lungs in rigid container, which has air tight seal (a), a pressure monitor (b), lung attachment (c), lungs (d), diaphragm (e), and contain a method for adjusting pressure in diaphragm (f).

2.1 Dismissal of Need for Tissue Fixation

Design of the needed ventilation chamber began by attempting to recreate the conditions of the chest cavity. One of the first considerations included discussion of tissue fixation, and whether or not it was necessary or optimal for testing. Fixation is used to preserve tissues after removal, in a life-like state which stops decomposition so that cellular processes that were underway just prior to removal can be viewed (Klatt 2014).

It was decided not to attempt fixation of the lungs for numerous reasons. First, the amount of tissue present would require a fixation procedure that could last for weeks, and as a ratio of 10:1 of fixative to tissue is recommended for ideal fixation, the amount of fixative needed would be immense (Klatt 2014). Typically, the optimum tissue size for

fixation would be no more than 5 mm thick, and no larger than a postage stamp (approximately 2 cm). In addition, fixing at this size can still take three to seven days (Randolph-Habecker 2012). Second, the process would undoubtedly end with uneven fixation as the outermost tissue would become fixed early in the process, making it difficult to judge progress of the interior tissue, and making it more difficult for the chemicals to reach the innermost tissue (Trachsel et al. 2011). Third, fixation would decrease the compliance of the tissue, therefore, the tracheal tissue would become stiffer than untreated tissue, and would not retain the same characteristics of tissue that stents would be in contact with after implantation.

There are protocols in "plastination" of tissue, but these would not be considered for these purposes, as this process solidifies the tissue, replacing water and fat with polymers such as silicone and epoxy, resulting in a solid piece that would not contract and expand with ventilation (von Hagens et al. 1987). In addition, with plastination, the tissue would become less likely to be damaged; whereas this is an important variable to consider during stent deployment, as if tearing of the tissues occurs with an excised lung, damage in live tissue would definitely be expected. Because this damage leads to granulation, which can advance to the point of blocking air flow into the lungs, potential to damage tissue would remain an important variable to consider. As porcine lungs can be obtained fairly cheaply from a slaughterhouse, it was accepted that fresh lungs would be purchased as needed for measurement and testing.

2.2 Proof of Concept and Material Selection

To begin the design process, many types of chambers were researched and considered. The first step of the design process required a proof of concept that negative

pressure could be obtained in a rigid chamber; a square box was obtained, not large enough for testing with actual lungs, made of acrylic with 12.7 mm (0.5 in) diameter, and pressure was applied to a rubber diaphragm sealed to the top of the chamber. Pressure was applied via a compressor, which immediately indicated that a smoother, steady, and slower application of pressure would be necessary to replicate breathing. At the time, a vacuum was not available, although the sides of the chamber and lid noticeably bowed, indicating the chamber was under pressure.

Research was conducted to find a suitable chamber already on the market, which would be an appropriate size to fit snugly around porcine lungs and a diaphragm to provide minimum volume around the lungs, rigid as a rib cage would be, would be cost effective, and able to be sealed to prevent leakage of water or air when pressure was applied. A suitable chamber already on the market was not found. Therefore, it was determined that Lexan™ (polycarbonate), a rigid material, would be preferable to Plexiglas® (acrylic) as acrylic is more prone to shatter, although acrylic is less likely to scratch. In addition, polycarbonate is able to undergo a higher number of cycles in an autoclave, and better withstands the application of pressure, as it is virtually unbreakable. Both materials are able to undergo a process similar to welding, where methylene chloride is used to fuse the material together (Gore et al. 2014). Glass was also considered as a potential material, however, it would be likely to shatter easily in comparison, as acrylic is four to eight times stronger than glass, and polycarbonate is 200 times stronger. Additionally, glass would prove much more difficult for the Machine Shop to manipulate.

2.3 Evaluation of Early Design Concepts

Initially, a cylinder was desired for the body of the chamber, but there was difficulty finding a cylinder of ample size, to fit around the porcine lungs, which were found to have average dimensions of 45.72 cm (18 in) from the superior end of the trachea to the inferior portion of the lungs, 20.32 cm (8 in) of total lateral distance of both sets of left and right lobes, with a depth of 7.62 cm (3 in) across the frontal plane from ventral to dorsal. These averages were provided by the slaughterhouse, and verified once acquired. In addition to a cylindrical body, a lid that screwed onto the chamber was desired, to further ensure air and water leakage would be blocked. Many cylinders widely available were not large enough to house porcine lungs, were significantly more expensive than their sheet-made counterparts, or were made of flimsy materials, which did not follow the recommendations given to the Tracheobronchial Stent Design (TSD) team.

One early design, devised by Dr. Kolok and depicted in Figure 2.2, consisted of the use of a six and a half gallon glass carboy, with the bottom cut off, to allow for the diaphragm to be adhered. This design was rejected due to the difficulty cutting the bottom edge away, worry of sharp edges tearing the diaphragm and being dangerous to the operator, as well as difficulty adhering the diaphragm well enough to maintain a sufficient seal. In addition, the size seven stopper that the carboy uses, would not provide a sufficiently large surface for the addition of a barb to attach the lungs to. As the stopper has a top diameter of 37 mm (1.46 in) and bottom diameter of 30 mm (1.18 in), attaching a barb would have left little material in the stopper for support or other ports. The tracheal attachment barb would require approximately half of the bottom diameter to be drilled out,

as the base of the barb has a diameter of 27.15 mm (1.06 in). Also, adding ports to the chamber could be dangerous and more difficult than desired.

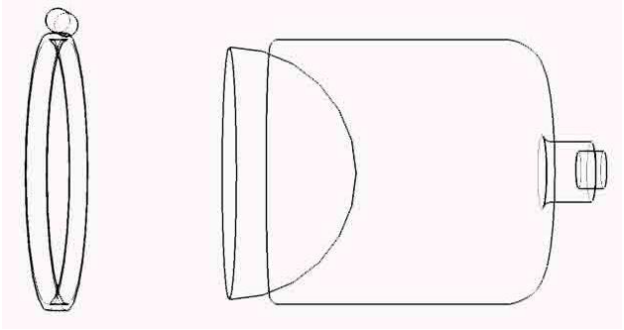

Figure 2.2. Ventilation Chamber Concept 1. Representation of glass carboy, cut at flat end to allow for attachment of diaphragm. Trachea proposed to be attached to rubber stopper, size 7.

The second concept design, depicted in Figure 2.3, had a large body for the lungs, with an angled side that narrowed to follow the form of the trachea. A plate surrounded by a gasket, with a cutout on the bottom that fit around the trachea, was proposed as a method to prevent fluid from leaving the body of the chamber, so that the trachea would not become filled with liquid. The advantages of this chamber included that it would be shaped to fit around the lungs and trachea, providing a tighter fit, as experienced in the ventral cavity; the chamber would be able to accommodate numerous ports, such as inlets and outlets for air or fluid; the diaphragm could be attached below the lungs, as shown, or attached to the lid, which could lift off for placement of the lungs in the chamber.

Additionally, the tracheal end of the chamber could be constructed at a downwards angle, which would follow the suggestions of previous work performed on rodents by von Bethmann et al. and Lilburn et al., which describe chamber placement on a 20° angle, creating 1 cm of height difference between top and bottom of chamber, and a design as "lung with orifice pointed down", respectively (von Bethmann et al. 1998; Lilburn et al. 2013). The disadvantages of this design include: complicated, unnecessary angles; also,

the plate cutout around the trachea would be hard to standardize, even with a strong yet compliant gasket to accommodate varying trachea dimensions, leading to leakage; and if the diaphragm was attached to the lid, in parallel with the lungs, this would interfere with the inflation of both the diaphragm and the lungs, as not much space would remain, although with diaphragm placement at the inferior end of the lungs, it would be more difficult to seal the diaphragm sheeting to the wall. Due to the over-complexity of this design, it was rejected with the goal of defining a simpler design.

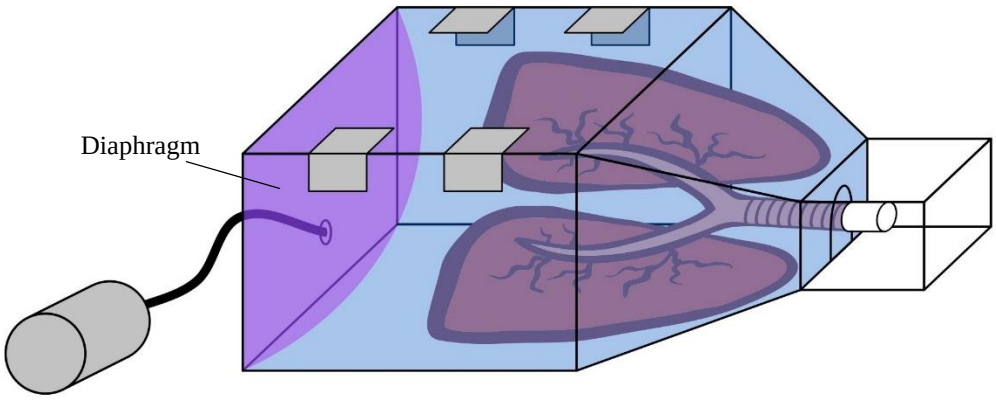

Figure 2.3. Ventilation Chamber Concept 2. Chamber with many angled portions, and removable plate that fits around trachea to block fluid.

A third design was devised with the assistance of Dr. Kolok, to be a square chamber, separated by a plate with holes at the bottom, with a plunger on one side, to act as a diaphragm, which is used to move fluid through the holes, while the lung sits on the opposite of the plate. An illustration of this design can be seen in Figure 2.4, below. This design would require an adherence area for the lungs, such as a barb that is open to atmosphere to be installed on the detachable lid, which would be simple to accomplish. Other ports could be added to the lid or walls easily as well, as it would be constructed of polycarbonate.

In the middle plate, holes would need to be drilled at the bottom to allow for fluid to be pushed and pulled by suction into and out of the side with the lung, causing the pressure difference. In favor of this design would be a simple to construct chamber, which allows for attachment of the trachea in a manner to prevent fluid from entering the lungs, and the use of a plunger which can be manually or mechanically controlled. The downsides of this design include difficulty ensuring the plunger can easily move enough in both directions to provide the needed pressure difference, as well as the difficulty continuing to control the plunger if it was deemed necessary to invert the chamber, as suggested previously. Additionally, the plunger would likely leak, as the corners would be difficult to seal, causing them to be susceptible to leakage. A permanently attached diaphragm would not be optimal, as this blocks the ability to clean the chamber. The idea was proposed to place pressure marks on the side of the wall, so that the displacement of fluid could be monitored, but it was decided that this would not provide an accurate gauge due to different lung sizes. This design was also rejected.

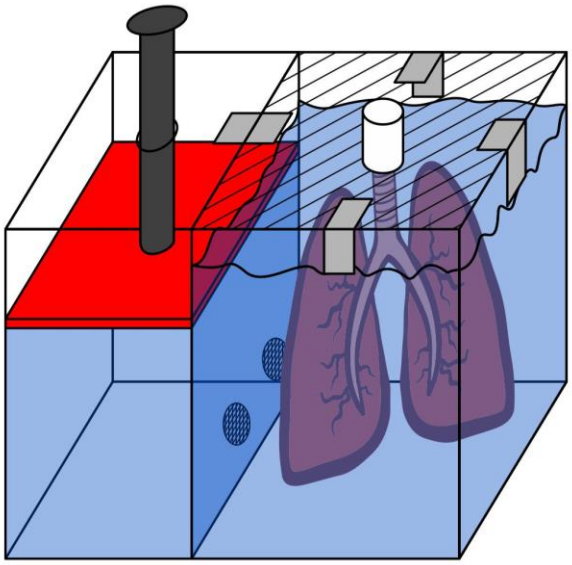

Figure 2.4. Ventilation Chamber Concept 3. Square chamber divided by wall, with holes in the bottom, to allow fluid flow between sections. Plunger would move to create pressure difference, and lungs would be open to atmosphere through attachment to lid.

In Ventilation Chamber Concept 4, the diaphragm is vertical, just as the lungs are, which does not fully mimic the body, but the chamber could potentially be rotated to lay with the trachea and lungs horizontal. With this particular design, the diaphragm would be attached on one side near the opening and closing of the lid, and also would be expanding beside the lungs, which both could potentially cause interference, as also discussed with Concept 2. The top lid would require a gasket, and would need to be clamped. In addition, without a release for fluid, the chamber could not be filled to capacity, although a port could be added if necessary. Optimally, a pump would control the diaphragm, which could be achieved by attaching a rod to the diaphragm, or by filling the diaphragm with fluid. Attaching a rod to the diaphragm presents more problems, as the most secure fit would likely result in having a hole in the diaphragm, which would lead to sealing issues.

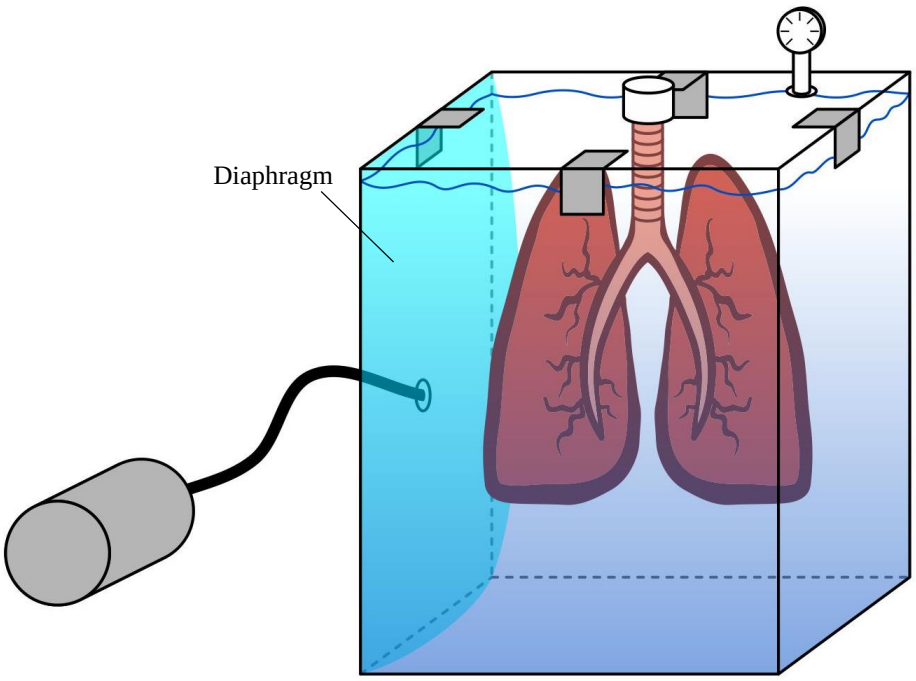

Figure 2.5. Ventilation Chamber Concept 4. Diaphragm placed parallel beside lungs, which are attached to lid and open to atmosphere. Gasket and clamps required around lid.

2.4 Choosing a Diaphragm

As the body uses a diaphragm to control the movement of air, a method of adding one to a ventilation chamber was needed. The diaphragm needs to meet the criteria of being air tight, water tight, and have a high compliance and tensile strength. Numerous materials were considered, before settling on a two tube latex bladder that is typically used in sphygmomanometers, more commonly referred to as blood pressure cuffs. Two sizes were obtained, with the specifications of: 20.32 cm by 6.35 cm (8.0 in by 2.5 in) for the smaller bladder, and 38.1 cm by 11.43 cm (15 in by 4.5 in) for the larger bladder when fully inflated. The bladders were estimated to be cylindrical when filled completely, and therefore, volume was estimated as:

$$V_{cylinder} = \pi r^2 h \qquad \textit{eq. 2}$$

Estimated volumes of 643.36 mL (39.26 in^3) and 3,778.20 mL (230.56 in^3) were calculated. The thickness of material was measured to be 0.82 mm (0.03 in) of both bladders. Figure 2.6 represents the chosen bladder used as a diaphragm. The two tubes were attached to the chamber via barb fittings, for inflation and deflation by pumps connected inline, on the exterior of the chamber.

A sheet of 1.5875 mm (1/16 in) ultra-strength silicone rubber was obtained from McMaster-Carr, and used in the initial testing. Although this material was compliant, for simplicity, further iterations of the design required a diaphragm such as the bladder. Problems sealing a rubber sheet to the chamber in a manner that would allow leak-proof, controlled air flow, which was also easily adjustable, showed that a sac-like diaphragm would be a better choice.

The smaller bladder was unable to provide pressure differences needed to replicate breathing in the lung. The larger bladder fared better, as it did affect the pressure of the chamber enough to allow the porcine lungs to inflate and deflate to accepted values similar to those experienced in humans, these results are further discussed in Chapter 5.

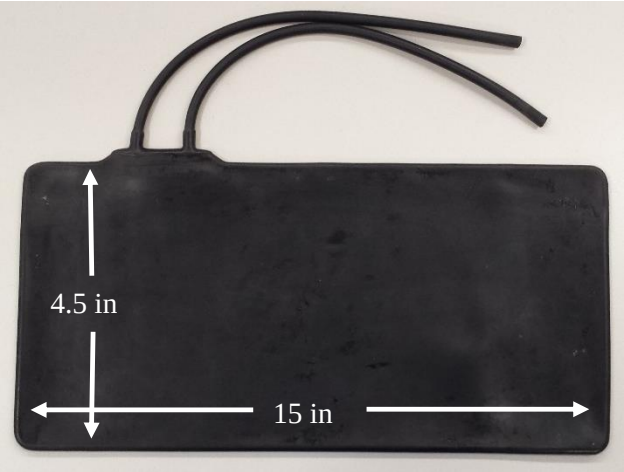

Figure 2.6. Two Tube Bladder Used as Diaphragm Substitute. Attached to pumps through barb fittings in the lid for inflation and deflation.

Other diaphragm materials were considered, such as an inner tube from a tire, a balloon, and 1/16" ultra-strength silicone rubber sheeting. An inner tube was purchased, but found to be much too rigid of a material, with very little flexibility. In addition, the material would not be pliable enough to allow itself to be easily manipulated in the chamber. A balloon was dismissed as a diaphragm due to doubts in the strength and durability of the balloon, and the nature of having to overcome the tensile properties of the balloon at rest before it expands; in addition to inconsistent elasticity over the course of many trials. Also, the bladder obtained allowed the greatest amount of flexibility in placement and adherence inside the chamber, which proved useful during testing of chamber prototypes.

2.5 Pressure Monitoring

In order to monitor the flow of air into and out of the lung, a spirometer was attached to the lid of the chamber, opposite the trachea. This setup allowed the trachea to remain open to atmosphere, as the mouthpiece allows gas to pass through a filament between the trachea and atmosphere. Spirometers calculate the volume of air inspired and expired by the lungs, so this is a useful test to determine if enough negative pressure is being applied by the diaphragm. A PASPORT Spirometer (PS-2152, Roseville, CA) by PASCO was used, with disposable mouthpieces of the Lilly type.

Lilly spirometers, also known as pneumotachometers, measure the difference in pressure before and after a membrane with known resistance. The Fleisch version is generally accepted to be more reliable, as they measure the difference in pressure through a series of parallel capillaries, though for the data required to monitor flow into and out of the trachea and lungs to atmosphere, as desired by the project sponsor, the Lilly type is acceptable. Both types rely on the Venturi principle that gas particles accelerate as their flow zone is reduced (Brown et al. 1986; MacIntyre et al. 2005).

The preliminary designs contained methods to monitor the pressure inside the chamber, which was not incorporated into the final design, as the spirometer was able to distinguish flow into and out of the trachea, which is valuable. One such method was for a water column, for example, by attaching stackable manometer tubes from a lumbar puncture kit or a flexible tube, but as the size of the chamber grew, this method was discarded, as the focus moved to measuring the volume of flow into and out of the lung. Also, the original goal of the water column was to replicate the amount of pressure change that the body undergoes, which would be commensurate to 10 mL of fluid moved in the

body (McGuire et al. 2014). However, as the ventilation chamber does not hold the lungs as closely as the rib cage of the same body, the volume around the lungs would not be comparable between the two systems.

In the body, the pleural space normally contains approximately 0.1 mL kg^{-1} of fluid, such that greater than 7 to 14 mL is considered abnormal in humans. Additionally, the pleural sac is generally only 10 to 20 μm in width, which would not be achievable in the proposed designs (Sriram et al. 2008).

Chapter 3: Design Prototypes

The first and second constructed prototypes were developed from 6.35 mm (0.25 in) Lexan™ polycarbonate as rectangular chambers with a removable lid, held in place by two and four vertical hold-down toggle locking clamps (DE-STA-CO® 317-U), respectively, with an added rubber gasket to help seal the chamber. The first edition of the chamber, Prototype 1, pictured in Figure 3.1, proved to be oversized, with inner dimensions of 59.69 cm x 36.83 cm x 19.05 cm (23.5 in x 14.5 in x 7.5 in). Prototype 1 also contained a plate on the interior to adjust the usable space of the lung compartment. This design was quickly deemed too large, as the lungs had no support, and the bladder was unable to provide enough pressure difference to ventilate the lungs.

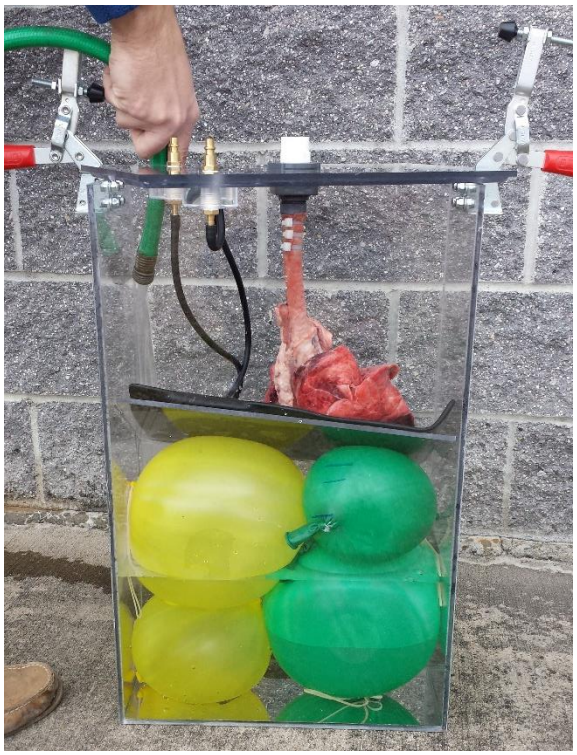

Figure 3.1 Image of Prototype 1. Balloons present to fill excess space.

A smaller chamber was subsequently constructed, Prototype 2, with inner dimensions of 36.83 cm x 25.40 cm x 8.89 cm (14.5 in x 10.0 in x 3.5 in), which fit much more tightly around the lungs, particularly in the smallest dimension. The lid of both Prototype 1 and Prototype 2 housed three ports: conduit for connection of trachea to chamber, and two fittings to attach the two tubes of the diaphragm on the inside of the lid, and for connection to the pumps on the outside of the chamber. The ports utilized plumber's tape and aquarium grade silicone to deter leakage.

Figure 3.2 is an image of Prototype 2 with the proposed plate, clamps, bladder, and tracheal barb visible. A valve was also added to allow for addition of fluid when lid is already in place. This is particularly useful when the chamber is tilted horizontally. These features are discussed in more detail following the image.

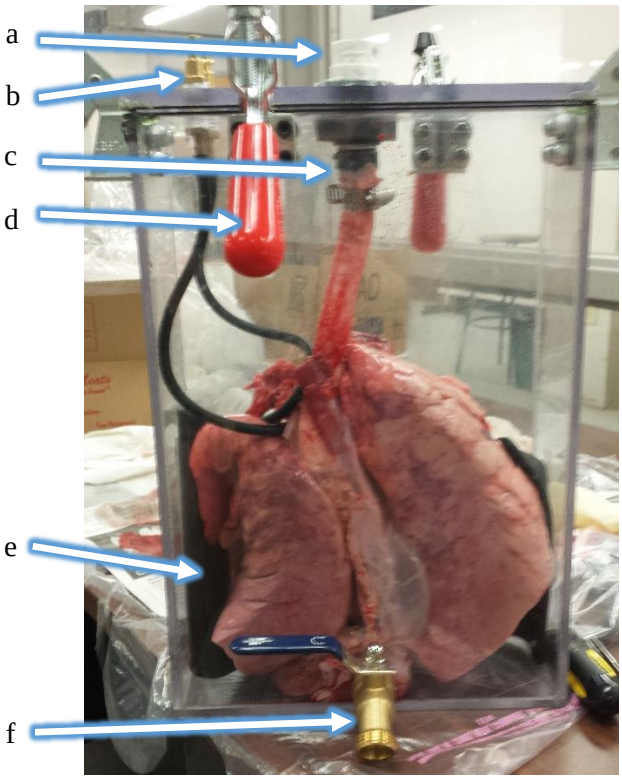

Figure 3.2. Image of Prototype 2. (a) Spirometer attachment piece, (b) fittings for pump attachment and tube attachment from bladder, (c) trachea attachment barb, (d) clamp to close chamber, (e) bladder, (f) valve to allow adjustment of fluid inside chamber.

The barb fitting for the trachea had dimensions of 3.37 cm (1.32 in) in length, and 14.28 mm (0.56 in) in width, which allowed for attachment with minimal restriction to the potential for air flow into and out of the trachea to atmosphere, as the larynx was removed from the lung sets. Opposite the tracheal barb, the spirometer was attached, with the outflow side of the mouthpiece attached to the lid, and the side normally reserved to be sealed by the lips, which is slightly smaller, left open to atmosphere. This direction was important and kept consistent so the sensor would not report values opposite to the actual flow, and would replicate normal use of the sensor.

Additionally, the rubber diaphragm was positioned and adhered to the chamber in a few different ways, for optimization of the design. For one iteration, the bladder was adhered to one of the large sides of the chamber, at the bottom. In another iteration, the bladder was adhered only to the short edges of the chamber, in an effort to allow one lobe of the lung on either side of the bladder, as the lobes appeared to be weighing down the bladder in the previous arrangement. As the bladder would occasionally not return to its natural shape, a horizontal plate was proposed to separate the bladder from the lungs. Prototype 2 was not large enough to allow for this configuration with a lung in place, so the design was tested with a balloon, and showed great promise. The next prototype was developed with the addition of the plate as a consideration.

For Prototype 2, the DE-STA-CO clamps were added to the middle of the two short edges, as well as on the long edges, offset, with one on either side of the centered trachea attachment piece. The clamps on the long edge could not be centered due to interference with the spirometer and the horizontal arms of the clamps. These clamps were unable to apply pressure evenly on the lid and gasket, therefore, leakage remained a problem with

this design. In addition, the clamps would cause the walls of the chamber to bow outwards when pressure was applied, further disrupting the seal. As the goal of this design was to have the ability to invert the chamber when desired, similarly to the previous work by von Bethmann et al. and Lilburn et al., any leakage was not an acceptable solution. A second gasket was added around the edge in an effort to reduce leakage, which did help to reduce leakage, however, fluid from the lungs began escaping through the spirometer, which negates the potential to retrieve results, as the spirometer filament would become contaminated.

3.1 Final Prototype Design

Prototype 3 was developed based on the shortcomings of the prior two prototypes. First, the dimensions in the x and y planes became 54.61 cm x 34.29 cm (21.5 in x 13.5 in), which were more similar to Prototype 1; however, the depth was more similar to Prototype 2, at 10.16 cm (4.0 in), a half inch increase over its predecessor. Table 3.1 displays the progression of sizing for the three chambers.

Table 3.1 Inner Dimensions of Prototypes in Relation to Average Lung Size

	Height (X)	Width (Y)	Depth (Z)
Average Size of Lungs	45.72 cm (18.0 in)	20.32 cm (8.0 in)	7.62 cm (3.0 in)
Prototype 1	59.69 cm (23.5 in)	36.83 cm (14.5 in)	19.05 cm (7.5 in)
Prototype 2	36.83 cm (14.5 in)	25.40 cm (10.0 in)	8.89 cm (3.5 in)
Prototype 3	54.61 cm (21.5 in)	34.29 cm (13.5 in)	10.16 cm (4.0 in)

Prototype 3, depicted in Figure 3.2, was developed to include a lid with an O-ring, which provided a more consistent seal than the previous design, as it fit the chamber similarly to a shoe box lid. In addition, smaller pull action latch clamps (DE-STA-CO®

323) were utilized, and placed evenly around the chamber, which held the lid in place securely. A plate was added 15.87 cm (6.25 in) from the bottom of the chamber, to separate the diaphragm from the lungs, and the diaphragm tubes were attached to the wall below the plate. The plate is screwed in place to maintain each compartment, and prevent it from moving should the chamber be tilted or inverted. Attaching the tubes and pump hoses at the level of the diaphragm, below the plate, allows for increased maneuverability of the chamber, as the pump hoses do not become detached accidentally between trials as the lid is removed and replaced; also, they do not cause any interference if the chamber is inverted, which was observed in testing of Prototype 2. Additionally, the spirometer was attached by a 3D printed connector, attached to the exterior of the lid, opposite the tracheal barb.

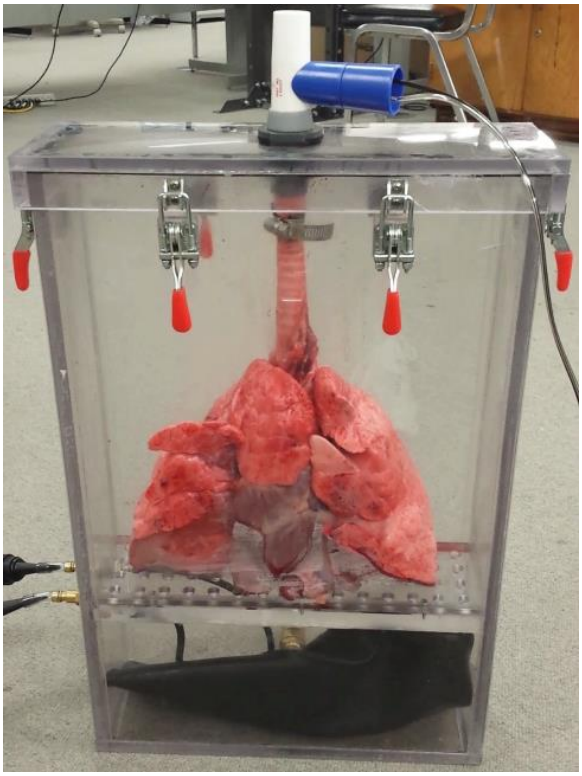

Figure 3.3. Prototype 3: Final Chamber Design. Clamps present, spirometer attached, gasket, bladder attached to box to act as diaphragm below shelf to protect diaphragm from interference by lungs, which are present.

Prototype 3 was constructed of thicker material than the previous two prototypes, to reduce flexing and bowing of the sides, as it is inherently more rigid. The polycarbonate chosen for this prototype is 9.52 mm (0.375 in) thick, whereas the previous chambers were constructed of 6.25 mm (0.25 in) thick material.

Chapter 4: Testing Procedures

Tests were first conducted of six human subjects to determine tidal volumes of real subjects, in an effort to verify similar volumes were achievable in the chamber (outlined in Section 4.1). Successful trials of box design were determined first by visual inspection, and secondly, by the total flow of oxygen into and out of the unobstructed lung, as measured by spirometer. In addition, flow rate data was obtained as obstructions were introduced to the excised porcine lung, to quantify the reduction of air flow in the presence of a stent or exterior force on the trachea.

Data was initially collected from a balloon acting as a lung proxy, as this provided a simple method to verify success without being wasteful with porcine lungs. Once reasonable success was obtained with the balloon, porcine lungs collected from Caughman's Meat'n Place in Lexington, SC were used for testing, and data was collected via the methodology discussed in Section 4.2.

4.1 Human Testing Methodology

The average tidal volume was calculated of six subjects, by use of a PASCO® PASPORT Spirometer with disposable mouthpiece, connected to the software PASCO® SPARKvue® (Roseville, CA). The spirometer was automatically detected, and the "build" option was used to create a graph that displayed time, in seconds, on the X-axis and Total Flow (L) on the Y-axis. A sampling rate of 50 Hz was chosen, and testing began.

The subject was asked to sit or stand comfortably, as well as, hold their nose during testing, so that all air exchange would pass through the filament of the spirometer. The

spirometer is held away from the mouth until the indicator lights on the sensor change from "Wait" (blinking red) to "Ready" (steady green). At this point, the subject places the spirometer in the mouth, and begins breathing normal, quiet breaths. The device should be between the teeth, with lips creating a seal around it. Each trial was one minute in length, after which, data collection was stopped, and exported for analysis. For accurate tidal volume estimation, the average of at least six breaths should be used (Quanjer et al. 1993); one minute trials provided more than enough breaths for estimation.

If the filament of the spirometer was contaminated during a trial, it was replaced for the subsequent trial, as contamination can increase resistance to air flow. Resistance could cause unrealistically high readings of flow rate and total volume.

4.2 Chamber Testing Methodology

Prior to testing and placement of the lungs in the chamber, the diaphragm must be connected by its two tubes to the ports in the chamber, and the diaphragm should be arranged so that it is stretched across the width of the chamber. Once the diaphragm is in place, the perforated plate should be screwed into place above it, so that the plate does not become displaced. In addition, the pumps are attached to the chamber.

Lungs were obtained from Caughman's Meat'n Place, which were requested with the trachea, heart, lungs, and diaphragm intact, and kept cool until ready for use. Before attaching the lungs to the chamber lid, the larynx was removed, as well as excess esophageal tissue attached to the trachea. The trachea was attached to the barb in the lid via a hose clamp, which was tightened around the outside of the trachea to keep it in place. The barb was also wrapped in silicone tape prior to lung attachment. Next, the lungs were lowered into the chamber, and petroleum jelly was added around the edge of the chamber

to help ensure a complete seal. Air was pushed directly into the lungs by a single bellows pump for two cycles of 0.5 L of positive pressure in an attempt to open the air passages, since surfactant was no longer being produced. The pump was not allowed to vacuum from the lungs for these two cycles, to keep the passages open. In normal breathing and forced exhalation, a subject would never fully empty their lungs of air, so the volume that remains is considered residual volume, and can be calculated by subtraction of the inspiratory vital capacity from the total lung capacity (Quanjer et al. 1993).

The chamber was then held open as the diaphragm (of the chamber) was inflated by two bellows pumps, each rated to displace 0.5 liters of air per depression of the pump. Once the diaphragm is inflated, initially to 1.0 L, the chamber lid is lowered and clamped in place. It is important to fill the diaphragm prior to sealing the chamber as the lung is initially in a resting position that is not considered inflated. Sealing the chamber prior to inflation of the diaphragm would cause the lung to decrease in volume further, limiting the potential for inflation as the alveoli collapse in an environment without surfactant production.

The spirometer mouthpiece is then placed into its connector on the lid, and measurement can begin; SPARKvue® software was used for data collection with the same set-up as for human testing. Breathing cycles were simulated by simultaneously pulling the pumps open, then pushing them closed, repeatedly, for one minute trials. As the pumps were pulled open by force, a vacuum is created in the chamber, causing the lungs to fill with air. Expanding the bellows also refilled the pumps with the air that would be used to re-inflate the diaphragm in the next cycle. Between trials, the hose was unscrewed from

the bellows in order to maximize the beginning capacity of the bellows, as they did tend to lose capacity throughout the trials.

Obstructions were recreated by either tightening a second hose clamp around the exterior of the trachea below the level of the barb, or by inserting a stent with a narrowed diameter. Stents were placed and removed by forceps. Images of these may be found in Section 5.2.3.

Chapter 5: Evaluation of Prototypes

Prototype 1 was deemed too large on visual merit, due to the difficulty of setting the adjustable plate and having an excess of space in the chamber. In addition, the lid did not stop leakage of air from the chamber, and the lungs were suspended without support, which is not representative of the body. It was determined the best course of action would be to scale down the chamber, resulting in decreased volume surrounding the lungs, which would better represent the thoracic cavity.

Prototype 2 was built to resemble the previous iteration, with the decreased dimensions discussed in Chapter 3. Preliminary trials were conducted with this chamber and a balloon attached as lung proxy, in an effort to determine if average flow rate increased in the presence of a high or low fluid filled environment. From visual tests, it was easily determined that the lung proxy performed better in a low fluid environment. Data collected from lungs in this prototype produced negligible flow into and out of the lungs, discussed in Section 5.2.1, therefore, it was necessary to construct the third prototype.

Successful trials were achieved with the third prototype, of unobstructed and obstructed flow by stent placement and external compression. As seen in the following figures, it was difficult to maintain flow throughout the course of each trial, which is due to the rudimentary nature of the pumps used. As the bellows ability to vacuum was reliant on the operator's strength and speed of pulling the bellows open, there was an overall decrease in pressure as trials progressed. Because the bellows failed to vacuum completely, each subsequent cycle was likely to have a reduced amount of flow into and out of the

diaphragm. Nonetheless, successful trials were still achieved, and average tidal volumes were determined, and compared to the human subjects.

5.1 Results of Human Respiration Tests

Tidal volume (TV) is considered a static volume, although it can be affected by numerous factors, including level of physical activity, disease processes, and even measuring conditions such as rest and posture; 500 mL is typically used as the starting rate for an adult male (Quanjer et al. 1993; Grotberg 2009). Artificial ventilation often aims to recreate the necessary pressures for optimal gas exchange, and clinical practitioners will often ventilate based on a range determined by the patient's ideal body weight (IBW). Before a normal ventilation range can be predicted, the IBW must be determined from the subject's height. The Robinson equation for estimation of IBW was used for these trials, as it has been shown to provide a better estimation of healthy weight for men than other equations such as the Broca, Hamwi, Devine, and etc, described in Appendix B.1 (Shah et al. 2006). The listed formulas do not provide exceptional estimates for women, therefore, for simplicity, the Robinson equation for women was chosen to estimate IBW of the female subjects as well (Shah et al. 2006).

Robinson Equations:

$$IBW\ (men) = 52\ kg + 1.9\ \frac{kg}{inch\ over\ 5\ feet} \qquad eq.\ 3$$

$$IBW\ (women) = 49\ kg + 1.7\ \frac{kg}{inch\ over\ 5\ feet} \qquad eq.\ 4$$

Estimates for TV were then calculated based on the subject's IBW. There is discrepancy between medical practitioners on the best estimation tactic, so estimates were taken by multiplying the IBW by seven and ten to create a range that many practitioners would find acceptable (Ricard 2003; Deakin et al. 2010). Table 5.1 describes the tidal

ranges established based on the six subjects' heights, as well as the values calculated for each subject.

Table 5.1. Ideal body weight and tidal volume range estimation of six volunteer subjects.

Subject	Height (in)	inches over 5ft	IBW (kg)	x 7 (mL)	x 10 (mL)	Calculated TV (mL)
F1	60	0	49.0	343	490	484
F2	62	2	52.5	370	520	692
F3	63	4	56.6	396	566	566
M1	72	12	74.8	524	748	632
M2	73	13	76.7	537	767	612
M3	76	16	82.4	577	824	1,887

Tidal volumes were then calculated from the volunteers from the data collected by the method described in Section 4.1. In order to determine the TV, the maximum and minimum values of each expiration were obtained, and the difference was averaged. Representative graphs of each subject may be found in Figure 5.1, with graphs of each trial visible for all subjects in Appendix C. It was common for trials taken from a single subject to trend in different directions, as the subjects may inhale a consistently larger amount than exhaled for one trial, resulting in a positive trending graph, and do the opposite in the next trial. In this case, a larger exhale would have taken place than inhalation, resulting in a negatively trending graph. Of course for more even breathing, the graph appeared to stretch out horizontally without trending upwards or downwards too far. For the trials depicted in Figure 5.1, most trials trend down as the exhalation was larger than inspiration, but this was not the case for all trials.

Subjects were asked to perform three trials, and to ensure that the average volumes were consistent between these trials, statistical analyses were performed. TVs of each trial were first compared by analysis of variance (ANOVA), and if the p-value was found to be

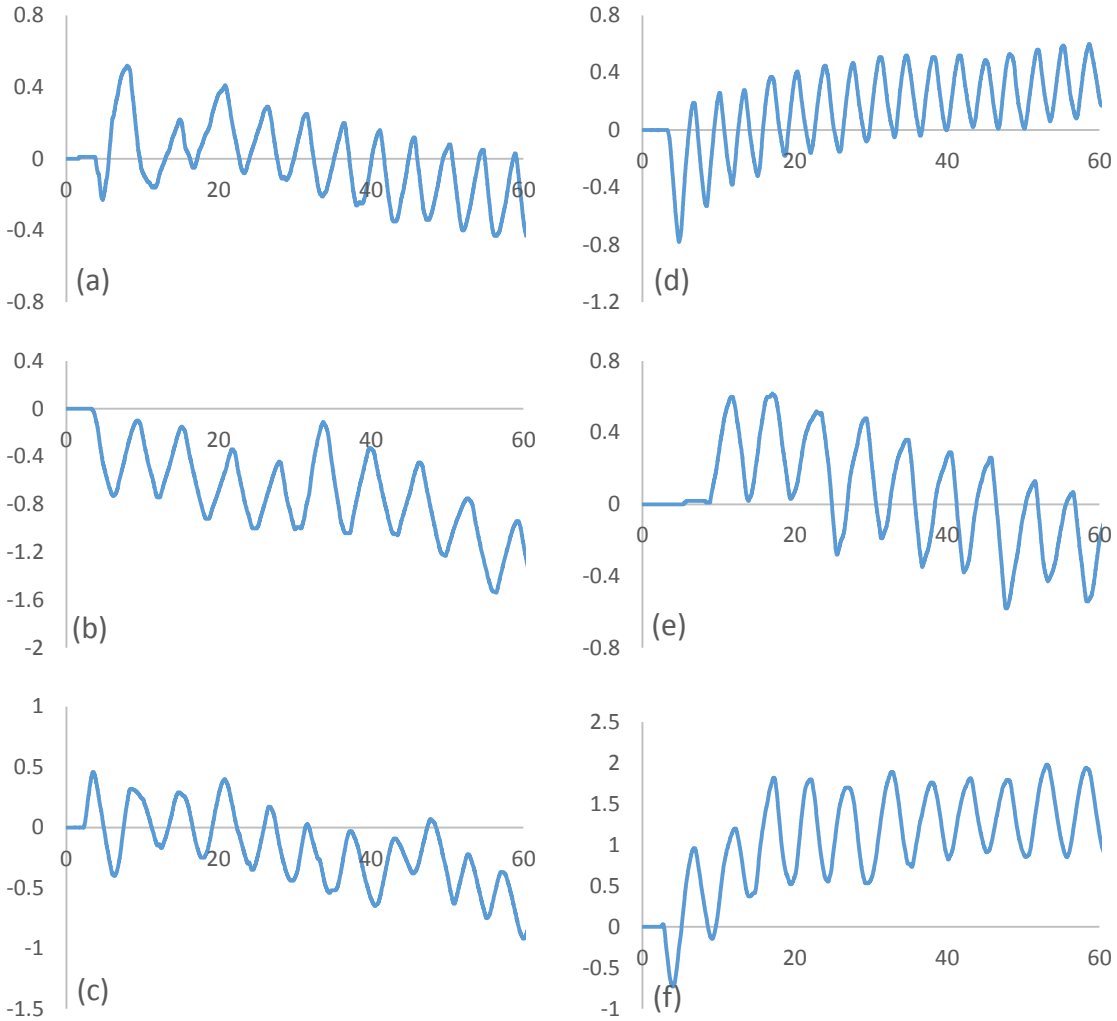

Figure 5.1. Representative charts of total flow (L) for quiet breathing of six subjects. Vertical axis of all is measuring total flow in liters, and horizontal axis is time in seconds. (a – c) F1, F2, F3; (d - f) M1, M2, M3.

lower than the alpha level of $\alpha = 0.05$ (95% confidence), then t-tests were performed between two trials at a time to determine which trial should be discarded from the overall average. P-values taken from these t-tests were analyzed according to the Bonferroni correction, which reduces the alpha level by the number of comparisons in order to avoid a Type I error of rejecting the null hypothesis when it is true (Information Technology Laboratory 2012). Therefore, because three trials were being compared, the p-value of each two mean comparison by t-test were compared to $\alpha = 0.016$ instead of $\alpha = 0.05$.

ANOVA analysis showed that F2, F3, and M2 produced trials that were similar enough to be considered equal at $\alpha = 0.05$, with p-values of 0.197, 0.705, and 0.080, respectively. The trials of F1, M1, and M3 produced p-values less than $\alpha = 0.05$, therefore, the null hypothesis that all average tidal volumes were equal was rejected. The ANOVA p-values of these subjects were 1.56E-13, 1.00E-3, and 1.93E-11, respectively. To determine which trial should be discarded, t-tests were conducted of these subjects' trials using the Bonferroni correction. For F1, Trial 2 vs Trial 3 was the only combination to produce a p-value above 0.016, with a two tailed $p = 0.416$. Because comparisons including the first trial produced p-values less than the alpha value, it was made clear that Trial 1 should be removed from further calculations. T-test comparison for M1 showed that Trial 1 should be removed as Trial 2 vs Trial 3 produced a p-value of 0.178, the only comparison larger than 0.016. For M3, the calculated p-value of Trial 1 vs Trial 3 was 0.023, the only combination of trials to produce a p-value larger than the alpha level. Due to this, Trial 2 was excluded from further comparison. A snapshot of p-values can be seen in Table 5.2, with full ANOVA and t-test results (as needed) located in Appendix D.

Table 5.2. Trial comparison p-values of each subject. ANOVA p-values are compared to α=0.05, whereas t-test p-values are compared to α=0.016, due to Bonferroni correction.

Subject	ANOVA P-Value	Trial 1 vs Trial 2	Trial 1 vs Trial 3	Trial 2 vs Trial 3
F1	1.56E-13	6.93E-7	2.66E-7	0.416
F2	0.081	x	x	x
F3	0.705	x	x	x
M1	0.004	3.13E-4	0.006	0.178
M2	0.063	x	x	x
M3	0.001	0.286	0.006	.001

Average calculated TV for all subjects is presented in Table 5.1; the average TV of F1, F3, M1 and M2 fell within their expected ranges, at 465 mL, 566 mL, 618 mL and 596 mL, respectively. Subject M3 displayed an average TV of 1,887 mL, which was 1,063 mL

higher than the larger expected value, a 129% increase. The average TV value of F2 was larger than expected as well, with a value of 692 mL, which is 172 mL larger than the expected range, or, 33% larger than the highest expected value.

5.2 Porcine Lung Testing

As lungs obtained are likely to have varying dimensions and levels of deterioration due to the slaughtering process, the amount of volume change per set of lungs is difficult to standardize. Although, TV estimation for pigs is accepted to be within the range of 5.9 – 14.5 ml kg^{-1} (Hannon et al. 1989; Wiklund et al. 2010). Therefore, controlling the other variables, such as how the lungs, spirometer, and diaphragm are readied, as well as keeping the same pump operators, is the best action for creating a consistent testing environment. The possibility of obscure cuts obtained during lung retrieval is also a concern, as these will affect respiration attempts.

5.2.1 Prototype 2: Evaluation of Performance

As previously stated, the lungs were inflated via positive pressure for two cycles, prior to experimentation with negative pressure to help open some air passages. The opening of the airways helped to create residual volume in the lung, so that the lung would be more accepting of passive inflation since the passages were more recently opened, with the goal of replicating the effects of surfactant production to some extent. The following figure (5.2) is a representation of the flow rate into and out of a lung in Prototype 2. The first trial produced some pressure difference, with a maximum flow rate of 0.25 L s^{-1}, resulting in a maximum tidal swing of 0.27 L, depicted in Figure 5.3. However, it was determined that the chamber was leaking, and the data was not able to be reproduced in later trials. In Trial 2, acting as a representative of further testing, taken once the chamber

was sealed, only negligible flow rates were obtained, with a maximum flow rate of 0.06 L s^{-1}. In addition, there was no evidence of tidal waves as a result of the negligible flow. As the chamber was sealed at this point, it was clear that this prototype would not produce results comparable to human respiration.

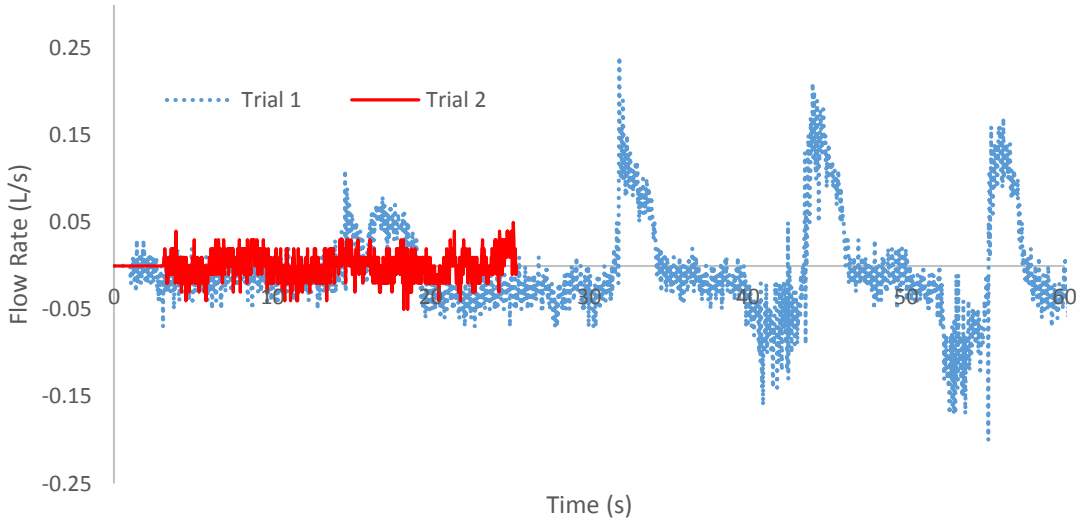

Figure 5.2. Flow rate of lungs in Prototype 2. Trial 1 produced flow rates as large as 0.25 L s^{-1}, although leakage was evident in the chamber. Trial 2, which was conducted after seal was improved, resulted in nearly negligible flow, with amplitudes averaging 0.06 L s^{-1}.

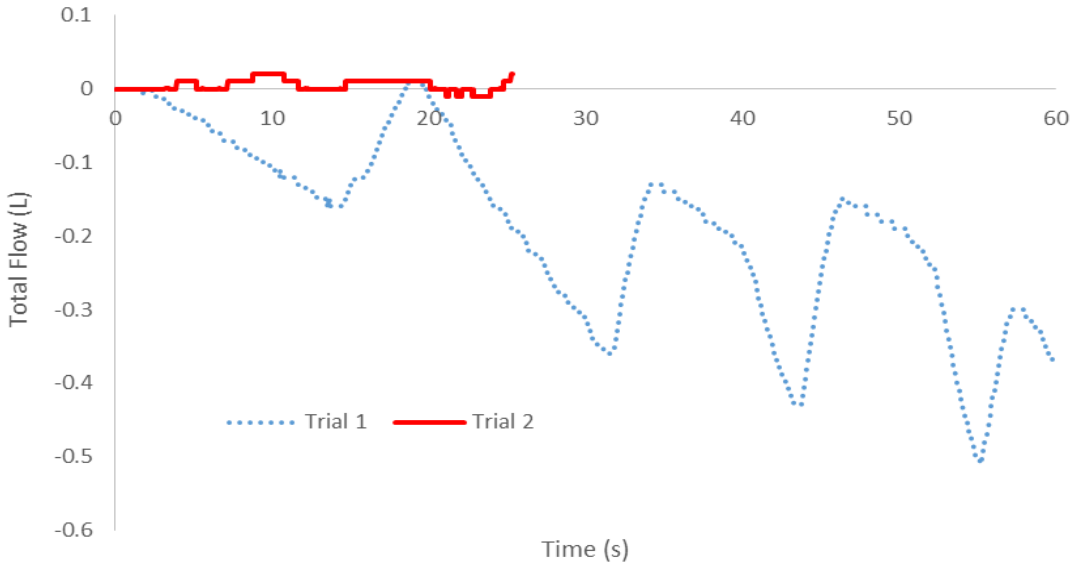

Figure 5.3. Total flow into and out of lungs in Prototype 2. Trial 1 does display tidal swings, with a maximum amplitude of 0.27 L. However, the chamber was found to leak. Trial 2 underwent negligible increases and decreases in flow, while the chamber was sealed.

5.2.2 Prototype 3: Evaluation of Ventilation without Obstruction

With lungs placed in Prototype 3 from a pig of between 90.72 – 136.07 kg (200 – 300 lbs), an average unobstructed TV of 982 mL was obtained from three trials, after ANOVA analysis to verify similarity between trials ($p = 0.608$ obtained). The TV produced also reached and exceeded a range similar to that of most people, therefore, Prototype 3 is considered successful in meeting the goal of reproducing human like pressure differences in the lung by negative pressure ventilation. Additionally, the TV achieved falls within the range expected based on the approximate weight of the pig and the multiplication factors of seven and ten. The lowest expected volume based on 90.72 kg equals 635 mL; whereas the highest expected volume based on 136.07 kg is 1,360 mL. Figure 5.4 presents total flow for the third trial, which also produced the largest tidal volume of the three trials. Figures for all trials may be found in Appendix E.

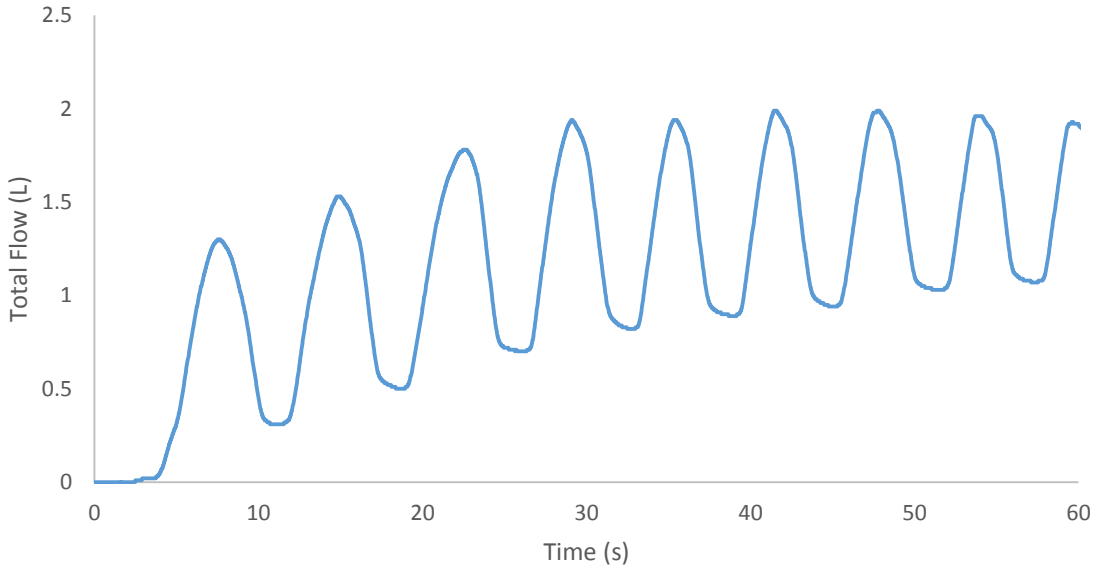

Figure 5.4. Trial 3 of unobstructed large lung in Prototype 3. Average tidal volume achieved of 1,013 mL for this trial.

A second set of unobstructed trials were also conducted of lungs obtained from a pig weighing approximately 77 kg (170 lbs). Using the method previously described to

estimate an acceptable TV range, volumes between 539 mL and 770 mL would be expected. Three trials were conducted, and an average TV was obtained of 579 mL from the first two trials, as Trial 3 was shown to be significantly different from the first two trials through ANOVA and t-testing. Table 5.3 provides p-values of all trials conducted with pig lungs, to include open airways and intentionally restricted airways. Figure 5.5 depicts the flow for the first trial, which produced the greatest TV of this set at 587 mL. Additional figures are located in Appendix E.

Table 5.3 Trial comparison p-values of porcine lungs. ANOVA p-values are compared to α=0.05, whereas t-test p-values are compared to α=0.016, due to Bonferroni correction.

Subject	ANOVA P-Value	Trial 1 vs Trial 2	Trial 1 vs Trial 3	Trial 2 vs Trial 3
Pig 1 (200-300 lbs)	0.608	x	x	x
Pig 2 (170 lbs)	1.64E-05	0.508	3.17E-05	3.59E-04
Pig 2 Open Stent	0.058	x	x	x
Pig 2 Clamped	7.30E-07	0.229	0.001	1.06E-06
Pig 2 Restrictive Stent	0.569	x	x	x

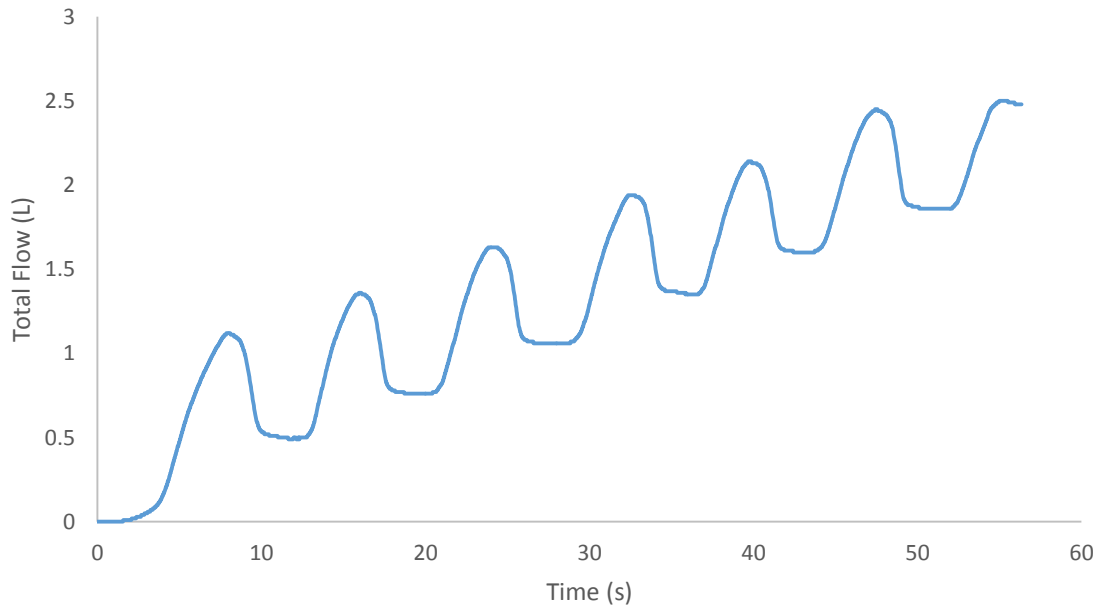

Figure 5.5. Trial 1 of unobstructed smaller lung in Prototype 3. Average tidal volume achieved of 587 mL for this trial.

Additionally, a stent with a wall thickness of 2.0 mm was 3D printed of VisiJet® SL Tough material, and placed in the trachea of the lungs harvested from the 77 kg (170 lb) pig to determine if its presence would affect respiration. In practice, this material would not be chosen for deployment in a human airway, as it does not exhibit properties conducive to implantation, in part due to its rigid nature. The piece was 50 mm (1.97 in) in length, with an inner diameter of 17 mm (0.66 in). The outer diameter of 19 mm (0.75 in) was slightly larger than the interior of the trachea, so once in place (possible due to the elasticity of the trachea), it fit snugly and ensured the trachea remained open. An average TV of 716 mL was obtained from three trials ($p = 0.058$), which resulted in an increase of 137 mL, or 23.7% over the same lung without the stent in place.

The estimated average number of breaths per minute for adults is generally listed to fall within the range of 8 to 20 breaths per minute (Dugdale III et al. 2013; American College of Emergency Physicians Foundation 2015), and all volunteers fell in this range. Between the two sets of porcine lungs, an average respiration rate of 7.2 breaths per minute was achieved, meaning that currently, the chamber is capable of producing flow rates similar to humans, although it does remain right outside the lower range. A more efficient pumping system would likely be able to increase the respiratory rate to fall within the range.

5.2.3 Prototype 3: Evaluation of Ventilation with Introduced Obstruction

Next, trials were conducted of the lung with obstruction, which was caused by two separate mechanisms: exterior compression due to clamp placement, and insertion of restrictive stent into the airway.

To create exterior compression on the trachea and reduce the inner diameter, a hose clamp was tightened around the trachea, to create a reduction of approximately 30% of the

outer diameter, resulting in a decrease to nearly 12.6 mm (0.49 in) from 18.0 mm (0.71 in). Figure 5.6 depicts the second hose clamp tightened around the trachea below the barb. Three trials were conducted, and the average TV fell to 467 mL based on Trial 1 and 2, as Trial 3 was seen to be significantly different ($p = 7.30E-7$), from an unobstructed TV of 579 mL from the same set of lungs, a 19.3% reduction in flow. The total flow of these tests maintained similar structure as the unobstructed tests, albeit with reduced magnitude. Graphical representation may be found in Appendix G.

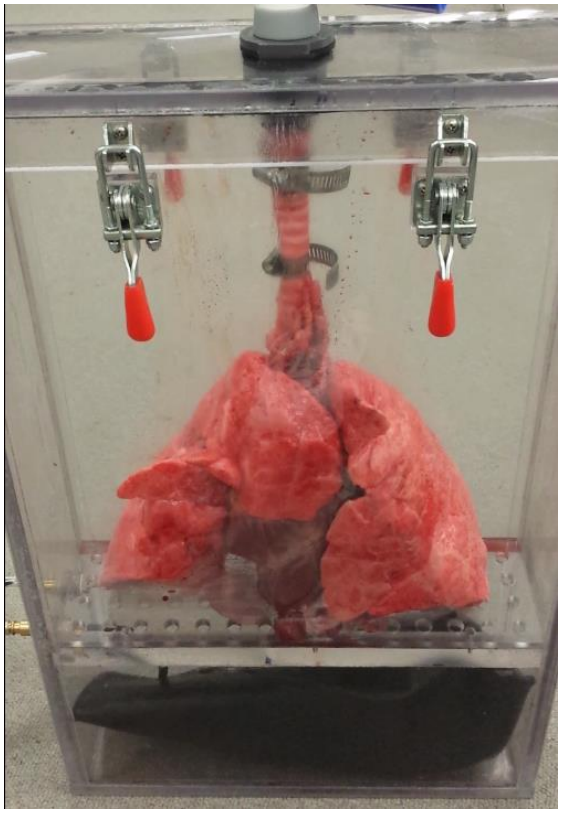

Figure 5.6. Image of hose clamp tightened around trachea. Clamp reduced the diameter by 30% due to external compression.

The interior obstruction was created by a stent inserted in the trachea, also printed with VisiJet® SL Tough material, which narrowed the inner diameter from the superior to inferior end to establish a 30% reduction within the stent. With this design, the inner diameter shrank to 13.0 mm (0.51 in) at the inferior end from 18.8 mm (0.74 in) at the

superior end, within a length of 50 mm. The following images show the reduction caused by the stent in the trachea, as it was excised after testing.

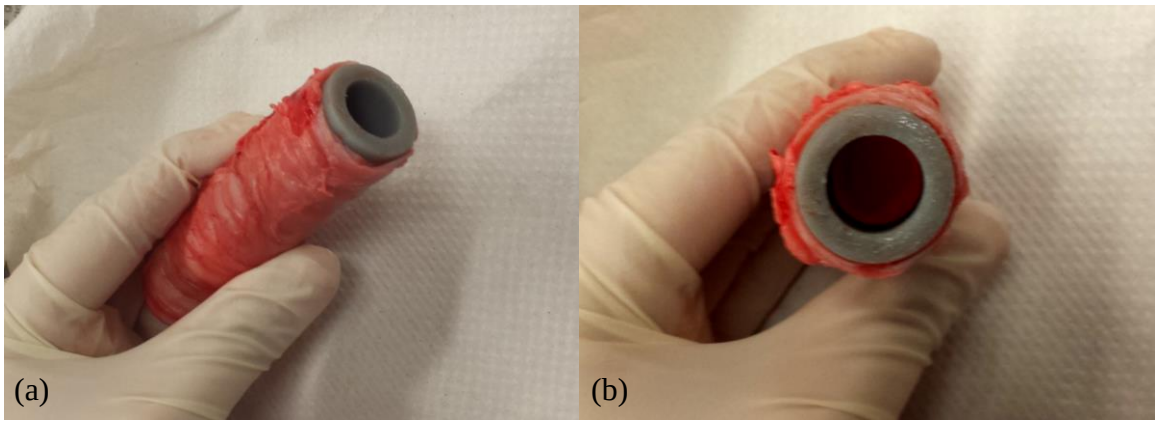

Figure 5.7. Trachea with 3D printed stent inserted to cause reduction by 30%. (a) Side view of trachea and stent. (b) Direct view of stent inside trachea.

Initially during testing, flow increased into and out of the lung, though the magnitude dropped off after the halfway point. The overall tidal volume for the three trials ($p = 0.569$) was 1,022 mL, though this does not reflect the sharp decline observed during the last breaths of each trial. For the first trial, a decline of 24% from the fourth to fifth peak was observed, and the reduced rate was maintained for the subsequent three breaths. For Trial 2, flow also began with an elevated flow, before a sudden decrease of 28% and 47% marked the final two breaths of the test. Trial 3 reacted similarly, showing four elevated breaths, which are followed by three breaths decreasing in amplitude by 30%, 11%, and finally, 13%, from each previous breath. Figure 5.7 (a) provides a graphical display of total flow for Trial 3.

The increase in flow for the first few breaths of each trial can be attributed to the increase in pressure that the stent caused by reducing, and essentially funneling air into the lung. This increased pressure helped to force open the airways more so than the passive intake of air experienced in an unobstructed airway, thus more air was able to initially fill

the lung with the stent in place. However, through the course of the trial, the pumps could not continue to produce the vacuum needed to remove air from the diaphragm due to air not escaping the lungs as easily. Hence, the pumps were unable to refill with air, so there was less air to push back into the diaphragm. Data depicting the flow rate (Figure 5.7 (b)), which was collected simultaneously with total flow, shows that later in the trials, the pumps were unable to achieve the flow rate seen earlier in the trial, which is consistent with the pumps being unable to push and pull air due to the restriction in the trachea. Had the trials continued, it is reasonable to assume that the pumps would eventually not be able to move enough air to cause any flow in the lungs, therefore, the total flow and flow rates would continue to shrink. Graphs of Trials 1 and 2 are located in Appendix G.

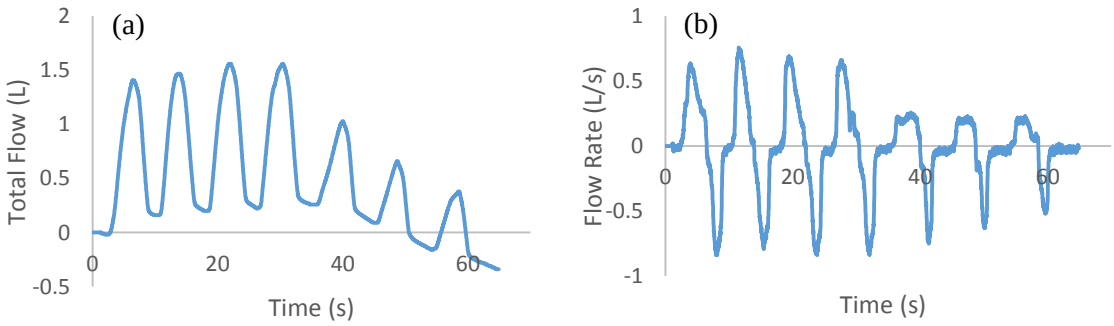

Figure 5.8. Reduction in magnitude of flow due to insertion of 3D printed stent designed with 30% reduction of inner diameter. (a) Total flow, (b) Flow rate.

It is also of note that the restriction in flow area also led to a slower breathing rate as it became more laborious to manipulate the pumps. For the three trials, only seven breaths were accomplished per minute; however, if trials were to continue for longer periods, it is likely the average would continue to decrease as it becomes more difficult to remove air from the diaphragm. An example of this can be seen with the final three breaths represented in Figure 5.8, as the average length of the breaths increased from 8.1 seconds

to 9.28 seconds, continually increasing with each breath. The elongation of breaths was present in the other trials obtained from the placement of the restrictive stent as well.

Chapter 6: Pump Selection

Currently, two Airhead high volume bellows foot air pumps are used to create the pressure needed to ventilate the lungs. Each pump has the ability to inflate and deflate, but under normal conditions, would typically only move air in one of those directions at a time. Normally, in order to move air in the opposite direction, the hose must be detached and screwed into the opposite port. Because the volume of two pumps was required to move into and out of the diaphragm at a given time, these pumps were modified to allow for them to pump and vacuum cyclically, without the hose being switched from inflate to deflate, and back again.

These pumps contained rubber flaps that would open during use to allow the "inflate" port to move air into a space, then the rubber flaps on the "inflate" side would close, blocking back flow into the bellows. As this occurred, the "deflate" side opened to fill the bellows from atmosphere. In order to allow the pumps to inflate and deflate without the need of moving the hose from one port to the other. Therefore, instead of changing ports, first, the flaps on the "inflate" side were clamped open, so that they were no longer blocking flow back into the bellows. Then, a piece was 3D printed for each pump, which screwed into the "deflate" port of the pump, to block the "deflate" port of each pump from filling the bellows from atmosphere. Figure 6.1 shows one of these pumps, with the 3D printed piece to block flow in place.

As the current method relies on operators manually opening and closing the bellows, an automated set-up is the logical next step in the attempt to produce consistency

between breaths and trials, which would also allow longer trials. In order to create the needed pressure and vacuum, a pump with a maximum flow of at least 8 liters per minute (lpm) should be considered, as each breath requires a flow rate of approximately 1 liter to inflate the lungs, as determined by averaging the amplitudes obtained from flow rate data of the open trachea porcine trials (average of 1.12 L obtained from three trials of the 170 lb pig's lungs without obstruction, figures in Appendix E). A pump with a maximum flow rate of at least 8 lpm will allow enough air to be available for each breath, while also allowing resources for a greater number of breaths each minute than the manual pumps were able to provide. In order to vacuum completely, a vacuum is needed that can meet the specifications of the given compressor.

Figure 6.1. Airhead® high volume bellows pump. Shown with 3D printed piece (gray) to block flow from "deflate" port.

6.1 Proposed Solution for Future Work

A compressor and vacuum pump were identified from Air Squared, Inc. The products suggested are P12H020A-BLDC-C scroll air compressor, and V12H020A-BLDC-C scroll vacuum pump, as these two are sister products, meaning the vacuum should

be able to vacuum at the same rate as the compressor pushes air (Air Squared 2015a; Air Squared 2015b).

The P12 and V12 compressor and vacuum both have variable speed, and have maximum flow rates of 20 lpm, which surpasses the minimum suggested of 8 lpm to achieve a life-like breathing rate. This pump also matches the maximum breathing rate considered normal by doctors, as previously discussed in Section 5.2.2. Additionally, the compressor contains a maximum pressure of 25 psi, which should be more than enough needed. The bellows pumps each had a peak air pressure of 2 psi, so it is reasonable to assume that a pressure in that range would continue to be adequate, although it may need to be slightly larger as the rate is increased, which is still within range of the chosen pump. Each pump is estimated to cost $1,250.00.

Because a cyclical flow is necessary, where the pumps are working opposite to each other, it is suggested that two controllers will be needed, such as the Moog BDQ-Q2-50-40 BLDC Controller, which is estimated at $365.00 each (Moog 2015).

Chapter 7: Conclusions

Three prototypes were developed in an effort to devise a chamber capable of recreating necessary pressure swings in order to ventilate ex vivo lungs by negative pressure. The final prototype was successful in ventilating lungs of two sizes in a manner that is repeatable and on par with the ventilation rate of humans. More specifically, the amplitude of total flow in porcine lung trials often exceeded the baseline set by the human trials, though with an automated pump system, these values can be decreased to match that of humans. In addition, the frequency of breaths was not statistically different from the baseline achieved by the human trials. Again, an automated pump system will allow for better control over this rate, and allow for an increase in breaths per minute.

The first step of testing was to obtain sample data from six human subjects with two goals in mind. The first goal was to determine the average tidal volume (TV) of each subject, subsequently verifying the accuracy of the estimated TV derived from the Robinson equation and multiplication factors of seven and ten, from the calculated ideal body weight for each subject. Calculated TV of four of the six subjects fell within the estimated range. This test was useful in determining if the lung volumes achieved from porcine lungs fell within the range achieved for humans, using the provided estimation method, outlined by Hannon et. al and Wiklund et. al. However, the caveat with this method of estimation is that ideal body weight of pigs for slaughter can't be exactly determined, as they are bred to be heavy, and lung volume doesn't change due to being over or under-

weight. Even so, for the purposes of this experimentation, the estimated TV range was based on the actual estimated weight of each pig.

The second goal was to determine repeatability using the spirometer, which was done through human testing. As was seen with the human testing results, there are many variables that can affect the output. Statistical tests to analyze similarity between the human trials showed that for three of the subjects, there was no similarity between their respective trials. Therefore, t-tests were necessary between each combination of trials to determine if any two were similar, using the Bonferroni correction. Porcine lung testing was not affected by a subject thinking and possibly manipulating their breathing pattern, so this variable was not present in the animal tests. Still, ANOVA was used to determine if rates varied widely between each set of porcine trials, and it was determined that just like the human trials, some cases of porcine trials showed significant difference, and thus could not be compared to one another.

Even with some trials appearing statistically different, the results still show that for the open trachea porcine lung trials, ventilation rates comparable to that of humans (which considers volume and breaths per minute) can be achieved; and in the restricted tests, ventilation does decrease over time. It was unexpected that flow would initially increase, however, as there was a decline in the amplitude of each breath towards the end of the trials, longer trials would be expected to continue this trend until flow became consistent once more, at a lower rate, provided a better pump and vacuum was utilized. The following table lists the average breaths per minute and TV achieved by each set of tests.

Table 7.1. Average breaths per minute (BPM) and calculated tidal volume (TV) for human and Prototype 3 testing.

Subject	BPM	Calculated TV (mL)	Subject	BPM	Calculated TV (mL)
F1	9.6	484	Pig 1 (200-300 lbs)	9.6	982
F2	9	692	Pig 2 (170 lbs)	6.6	580
F3	10.3	565	Pig 2 Open Stent	5.6	716
M1	17	632	Pig 2 Clamped	6.6	468
M2	10	612	Pig 2 Restrictive Stent	7.3	1,022
M3	12	1,887			

Lastly, a compressor air pump and vacuum pump were chosen as appropriate pumps to produce the necessary pressures to ventilate the lungs in the chamber. The P12 and V12 pumps by Air Squared, Inc. allow for a large enough maximum pressure and flow for continuing the testing outlined here, in a more precise manner. The pumps have variable speeds, with maximum flow rates of 20 liters per minute, which provide a large enough flow rate to achieve a breathing rate within the accepted range of 8 – 20 breaths per minute. Additionally, a Moog controller was identified which can control the cyclic pattern of breathing. Other pumps were considered, such as syringe pumps and bellows pumps, but none were identified to produce a large enough flow in the time needed. Syringe pumps can be linked, but these are typically responsible for much lower flow rates, and would be cumbersome to manipulate, as upwards of ten would likely be needed.

The final prototype was successful, therefore, it is ready to house lungs for the testing of more appropriate stents, as those tested here were either not sized properly, or not made of a viable material for insertion into the body. In addition, testing can evolve to include removing cartilaginous rings from the trachea, or by applying sodium hydroxide to the interior tracheal wall in an effort to recreate malacia, as a restrictive stent or exterior clamp would interfere with testing in a more life-like model. Furthermore, a perfusion

system could be added to the chamber, so that blood flow is recreated, as it flows through the heart and lungs.

Bibliography

Air Squared, Inc., 2015a. P12H020A-BLDC-C. Available at: http://airsquared.com/products/compressors/p12h020a-bldc-c/ [Accessed June 11, 2015].

Air Squared, Inc., 2015b. V12H020A-BLDC-C. Available at: http://airsquared.com/products/vacuum-pumps/v12h020a-bldc-c/ [Accessed June 11, 2015].

American College of Emergency Physicians Foundation, 2015. Emergency 101. *Emergency Care For You*, pp.1–10.

von Bethmann, A.N. et al., 1998. Hyperventilation induces release of cytokines from perfused mouse lung. *American Journal of Respiratory and Critical Care Medicine*, 157, pp.263–272.

Brown, M., Hammond, P. & Johnson, A., 1986. Pneumotachometer/graph. In *The Medical Equipment Dictionary*. London: Chapman and Hall Ltd.

Chin, C.S. et al., 2008. Airway stents. *The Annals of Thoracic Surgery*, 85(2), pp.S792–S796.

Costa, C. et al., 2013. Comprehensive molecular screening: from the RT-PCR to the RNA-seq. *Translational Lung Cancer Research*, 2(2), pp.87–91.

Deakin, C.D. et al., 2010. European Resuscitation Council Guidelines for Resuscitation 2010, Section 4. Adult advanced life support. *Resuscitation*, 81(10), pp.1305–1352.

Dozois, C.M. et al., 1997. A reverse transcription-polymerase chain reaction method to analyze porcine cytokine gene expression. *Veterinary Immunology and Immunopathology*, 58, pp.287–300.

Dugdale III, D.C., Zieve, D. & Black, B., 2013. Rapid shallow breathing. *National Institutes of Health: Medline Plus*, pp.1–3.

Estetter, R.H., Holland, T.D.J. & Higgins, J.T., 2005. Lung simulator. US Pat. 6,874,501 B1, pp.1–8.

Freitag, L. et al., 1994. Theoretical and experimental basis for the development of a dynamic airway stent. *European Respiratory Journal*, 7, pp.2038–2045.

Freitag, L., 2000. Tracheobronchial stents. *Interventional Bronchoscopy*, 30, pp.171–186.

Gore, M., Kolok, D. & Horton, C., 2014. Interview at USC School of Medicine February 27, 2014.

Grotberg, J.B., 2009. Respiratory mechanics and gas exchange. In M. Kutz, ed. *Biomedical Engineering and Design Handbook Vol. 1*. New York: McGraw Hill, pp. 95–123.

von Hagens, G., Tiedemann, K. & Kriz, W., 1987. The current potential of plastination. *Anatomy and Embryology*, 175(4), pp.411–421.

Hannon, J.P., Bossone, C.A. & Wade, C.E., 1989. Normal physiological values for conscious pigs used in biomedical research. *Division of Military Trauma Research*, pp.1–20.

Information Technology Laboratory, 2012. Bonferroni's method. In *NIST/SEMATECH e-Handbook of Statistical Methods*. pp.1–4.

Klatt, E.C., 2014. Histotechniques. *The Internet Pathology Laboratory for Medical Education*. pp.1-12.

Lilburn, D.M.L. et al., 2013. Validating excised rodent lungs for functional hyperpolarized Xenon-129 MRI. *PloS one*, 8(8), p.e73468.

MacIntyre, N. et al., 2005. Standardisation of the single-breath determination of carbon monoxide uptake in the lung. *European Respiratory Journal*, 26(4), pp.720–735.

Marquette, C.H. et al., 1995. Experimental models of tracheobronchial stenoses: a useful tool for evaluating airway stents. *The Annals of Thoracic Surgery*, 60(3), pp.651–656.

McGuire, F. et al., 2014. Group Discussion April 3, 2014.

Melgoza, E.L. et al., 2012. An integrated parameterized tool for designing a customized tracheal stent. *Computer-Aided Design*, 44(12), pp.1173–1181.

Moog, 2015. BDO-Q2-50-40. Available at: http://www.moog.com/products/motors-servomotors/brushless-motors/silencer-series-drive-electronics/bdo-q2-50-40/ [Accessed June 17, 2015].

Orden, B.B., 1979. Educational Lung Simulator. US Pat. 4,167,070, pp.1–7.

Quanjer, Ph.H. et al., 1993. Lung volumes and forced ventilator flows. *European Respiratory Journal*, 6, pp.5–40.

Randolph-Habecker, J., 2012. Tips about fixation and formalin. *Fred Hutchinson Cancer Research Center*. Available at: http://sharedresources.fhcrc.org/training/tips-about-fixation-and-formalin [Accessed January 15, 2014].

Ricard, J.D., 2003. Are we really reducing tidal volume - And should we? *American Journal of Respiratory and Critical Care Medicine*, 167(10), pp.1297–1298.

Saueressig, M.G. et al., 2011. Experimental model of tracheal stenosis with submucosal resection of cartilaginous rings combined with sodium hydroxide instillations. *Revista do Colégio Brasileiro de Cirurgiões*, 38(6), pp.412–416.

Shah, B., Sucher, K. & Hollenbeck, C.B., 2006. Comparison of ideal body weight equations and published height-weight tables with body mass index tables for healthy adults in the United States. *Nutrition in clinical practice : official publication of the American Society for Parenteral and Enteral Nutrition*, 21(3), pp.312–319.

Sriram, P.S., Antony, V.B. & Holm, K.A., 2008. Pleural effusion: how to confirm the cause and manage effectively. *Consultant*, 47(11), pp.1-5.

Thanawongnuwech, R. et al., 2004. Increased production of proinflammatory cytokines following infection with porcine reproductive and respiratory syndrome virus and mycoplasma hyopneumoniae. *Clinical and Diagnostic Laboratory Immunology*, 11(5), pp.901–908.

Trachsel, S. et al., 2011. High-quality lung fixation by controlled closed loop perfusion for stereological analysis in a large animal model. *The Journal of Surgical Research*, 166(2), pp.e97–e102.

Tripuraneni, S.C., Tripuraneni, S.C. & Kumar, N.S., 2012. Custom made acrylic tracheal stent for tracheal stenosis. *Indian Journal of Otolaryngology and Head and Neck Surgery*, 64(3), pp.298–300.

Uhlig, S. & Wollin, L., 1994. An improved setup for the isolated perfused rat lung. *Journal of Pharmacological and Toxicological Methods*, 31(2), pp.85–94.

Wiklund, C.U. et al., 2010. Influence of tidal volume on pulse pressure variations in hypovolemic ventilated pigs with acute respiratory distress-like syndrome. *Anesthesiology*, 113(3), pp.630–638.

Xing, Z. et al., 1997. Overexpression of granulocyte-macrophage colony-stimulating factor induces pulmonary induction of transforming growth factor-β1 and myofibroblast accumulation. *Americal Journal of Pathology*, 150(1), pp.59–66.

Appendix A: Patented Chamber Diagrams

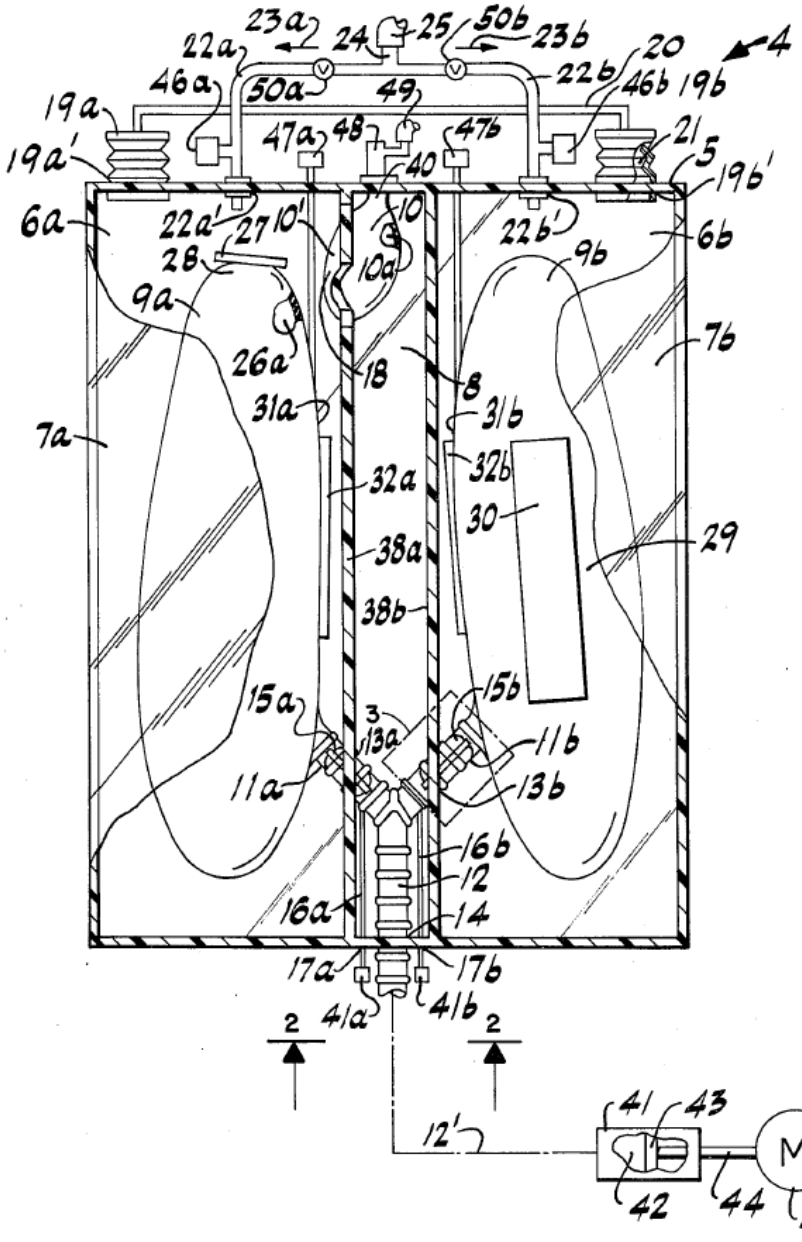

Figure A.1. Chamber design by Burt Orden, US Patent 4,167,070 (1979).

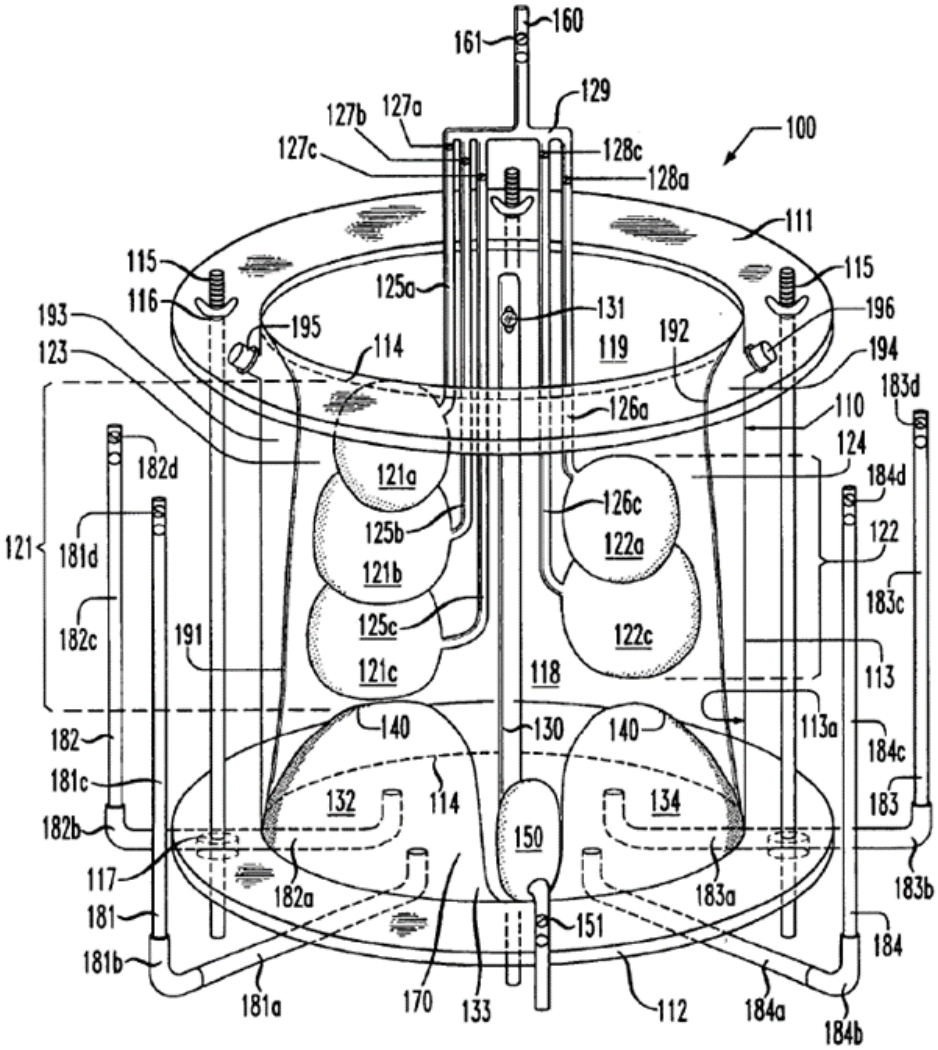

Figure A.2. Chamber design by Estetter et al., US Patent 6,874,501 B1 (2005).

Appendix B: Equations Used to Estimate Tidal Volume

Table B.1. Comparison of ideal body weight equations for men and women (Shah et al. 2006).

Source	Equation
Broca (1871)/H-index	IBW (kg) = height (cm) − 100
Hamwi (1964)[25]	IBW (men) =106 lb + 6 lb/inch over 5 feet IBW (women) =100 lb + 5 lb/inch over 5 feet
Devine (1974)[20]	IBW (men) = 50 kg + 2.3 kg/inch over 5 feet IBW (women) = 45.5 kg + 2.3 kg/inch over 5 feet
Robinson et al (1983)[19]	IBW (men) = 52 kg + 1.9 kg/inch over 5 feet IBW (women) = 49 kg + 1.7 kg/inch over 5 feet
Miller et al (1983)[22]	IBW (men) = 55.7 kg + 1.39 kg/inch over 5 feet IBW (women) = 53 kg + 1.33 kg/inch over 5 feet
Hammond (2000)[26]	IBW (men) = 48 kg for 150 cm + 1.1 kg/cm IBW (women) = 45 kg for 150 cm + 0.9 kg/cm

For Hamwi and Hammond, for a light frame, the calculated weight may be subtracted by 10%, and for a heavy frame, added by 10%. Miller et al formula is for medium frame.

Appendix C: Figures Pertaining to Human Ventilation Trials

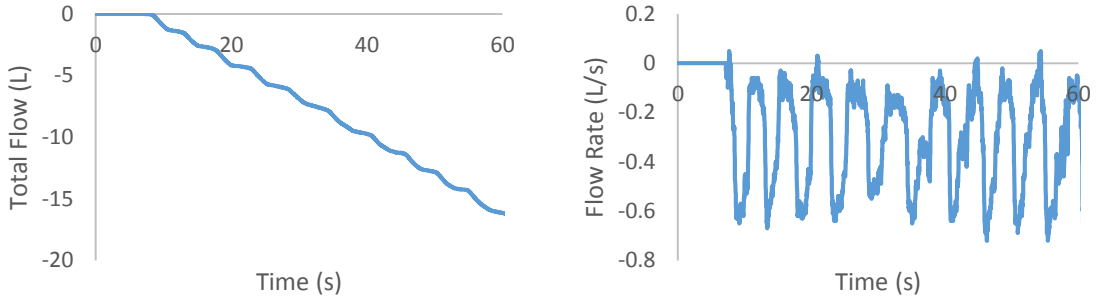

Figure C.1. F1 graphical representation of total flow and flow rate for Trial 1.

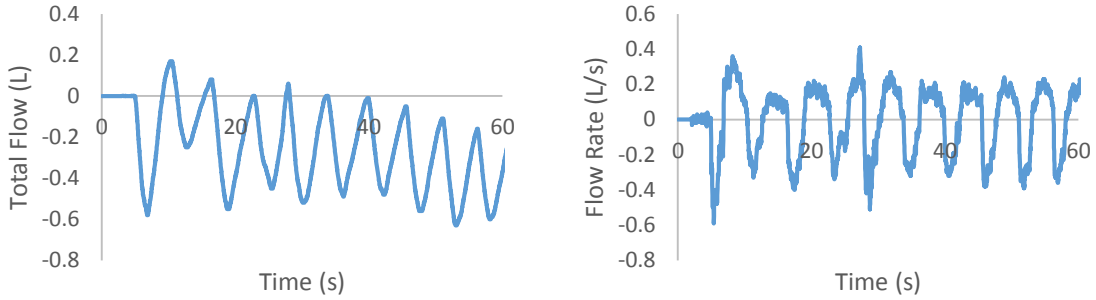

Figure C.2. F1 graphical representation of total flow and flow rate for Trial 2.

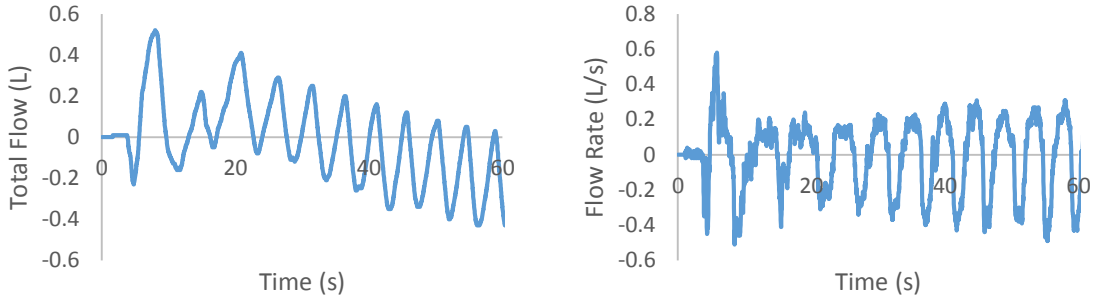

Figure C.3. F1 graphical representation of total flow and flow rate for Trial 3.

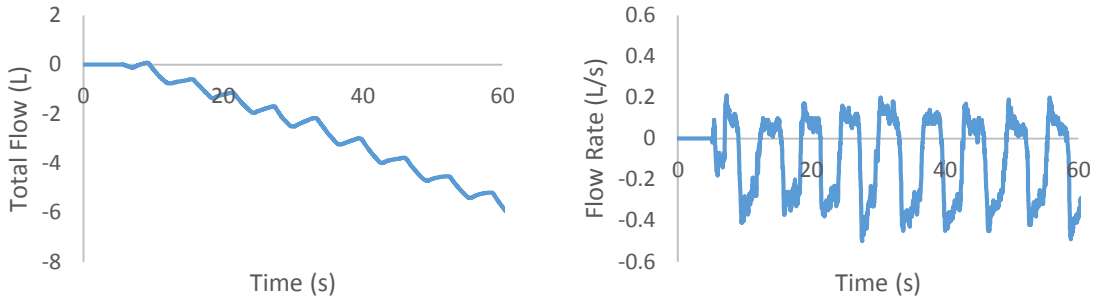

Figure C.4. F2 graphical representation of total flow and flow rate for Trial 1.

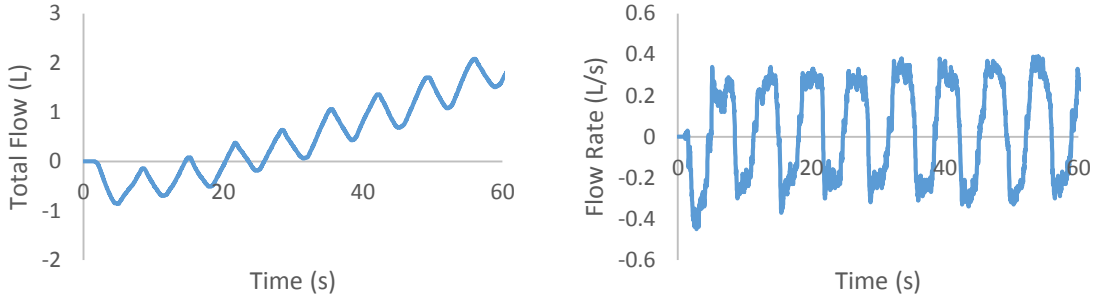

Figure C.5. F2 graphical representation of total flow and flow rate for Trial 2.

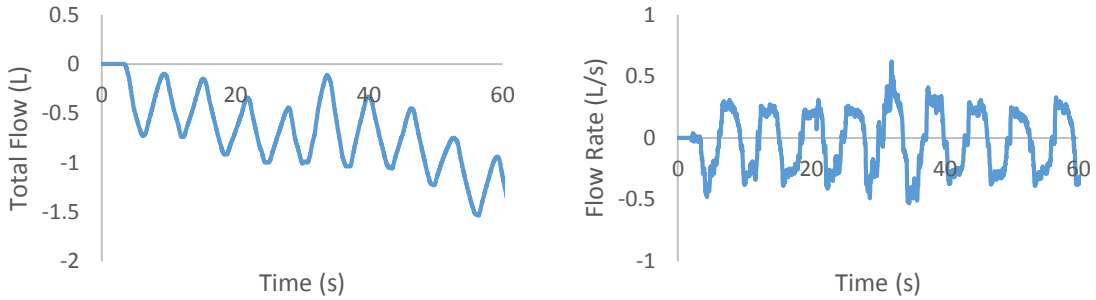

Figure C.6. F2 graphical representation of total flow and flow rate for Trial 3.

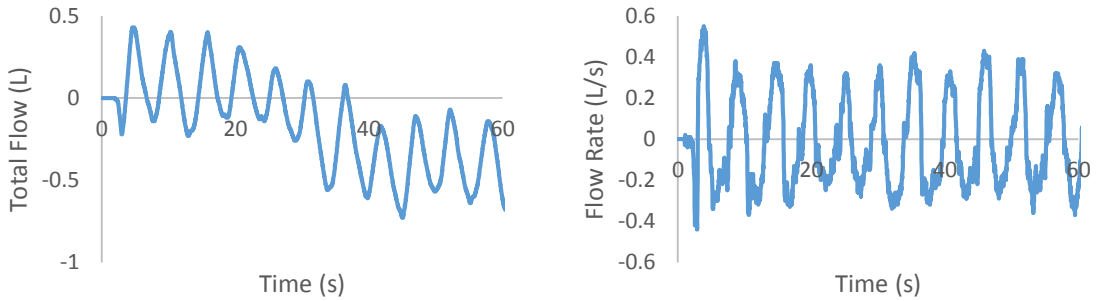

Figure C.7. F3 graphical representation of total flow and flow rate for Trial 1.

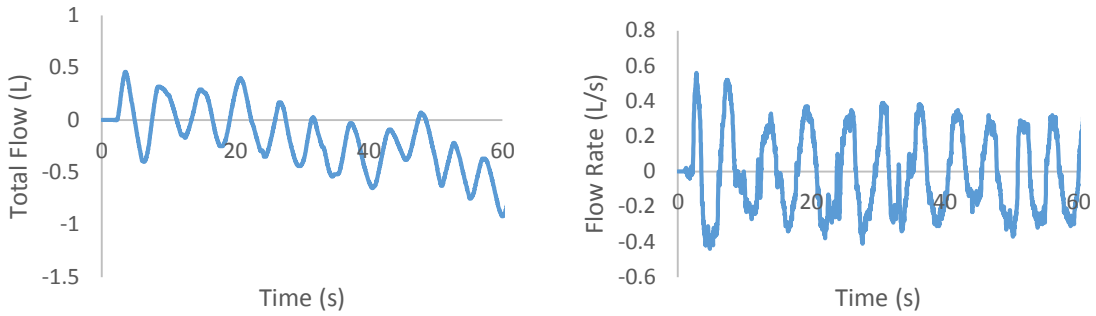

Figure C.8. F3 graphical representation of total flow and flow rate for Trial 2.

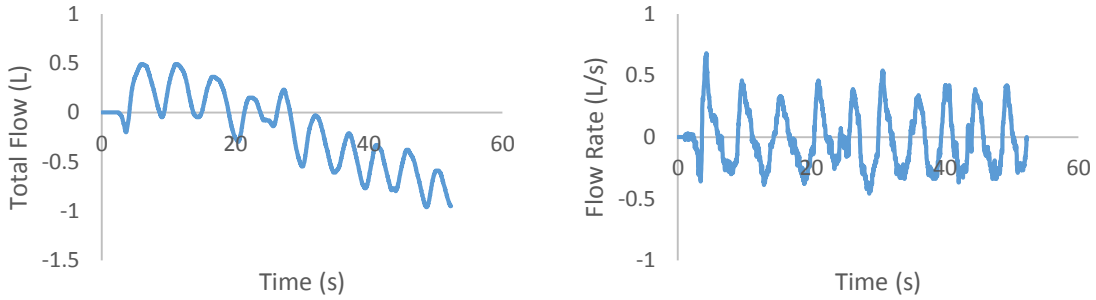

Figure C.9. F3 graphical representation of total flow and flow rate for Trial 3.

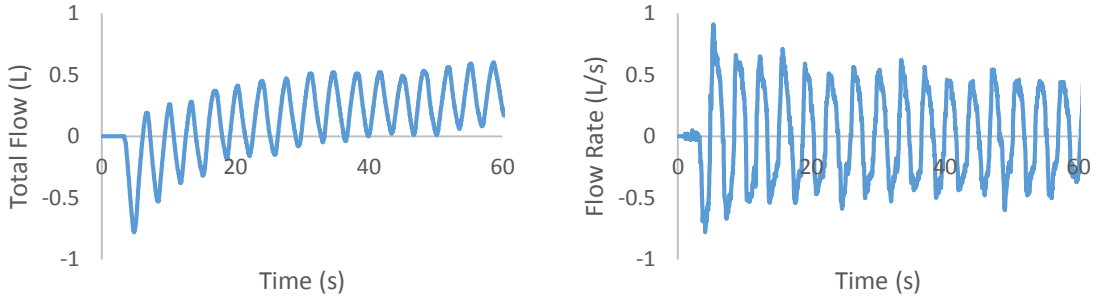

Figure C.10. M1 graphical representation of total flow and flow rate for Trial 1.

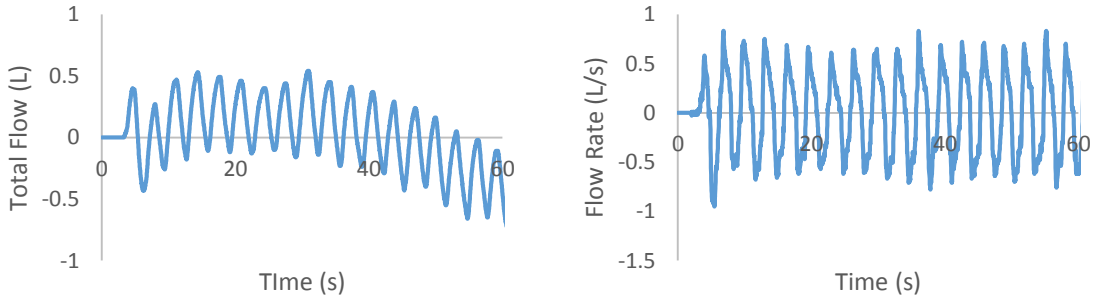

Figure C.11. M1 graphical representation of total flow and flow rate for Trial 2.

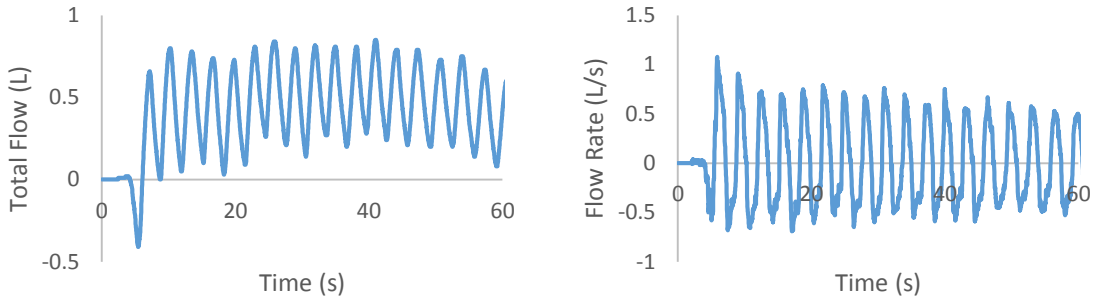

Figure C.12. M1 graphical representation of total flow and flow rate for Trial 3.

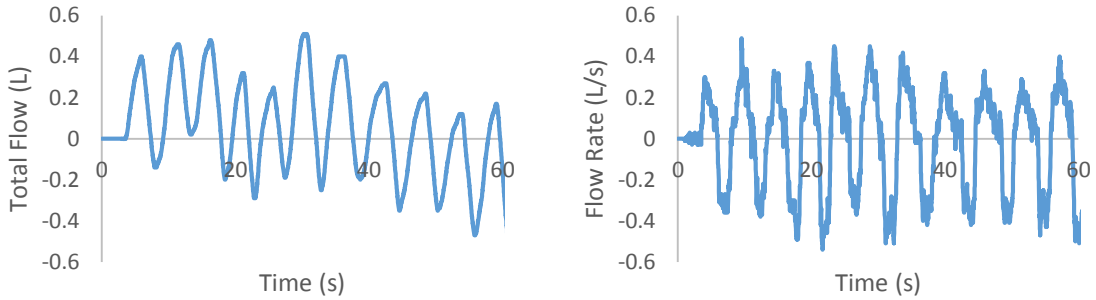

Figure C.13. M2 graphical representation of total flow and flow rate for Trial 1.

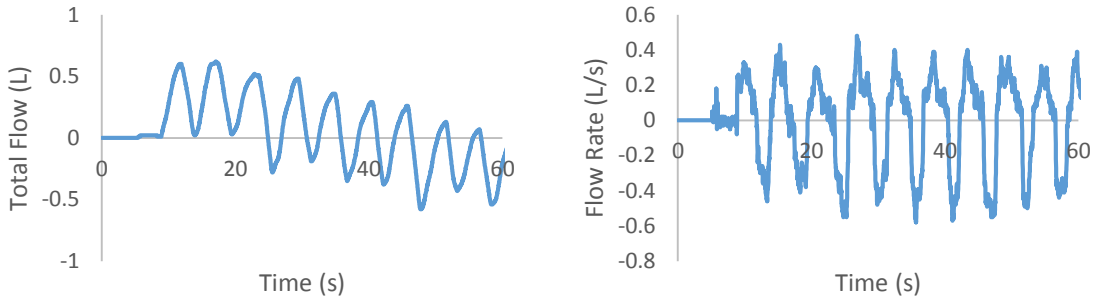

Figure C.14. M2 graphical representation of total flow and flow rate for Trial 2.

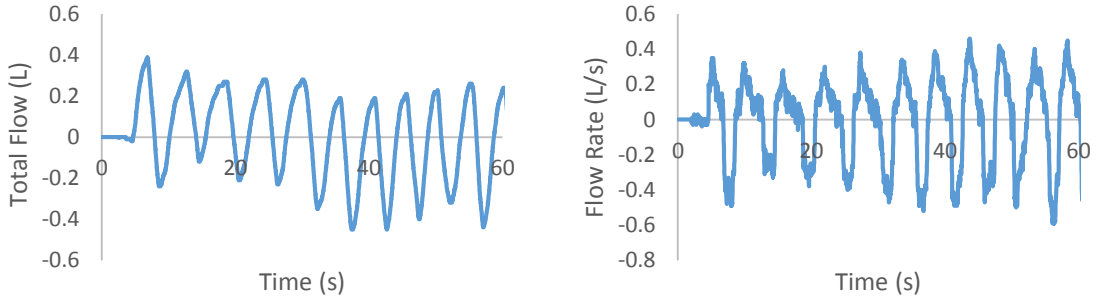

Figure C.15. M2 graphical representation of total flow and flow rate for Trial 3.

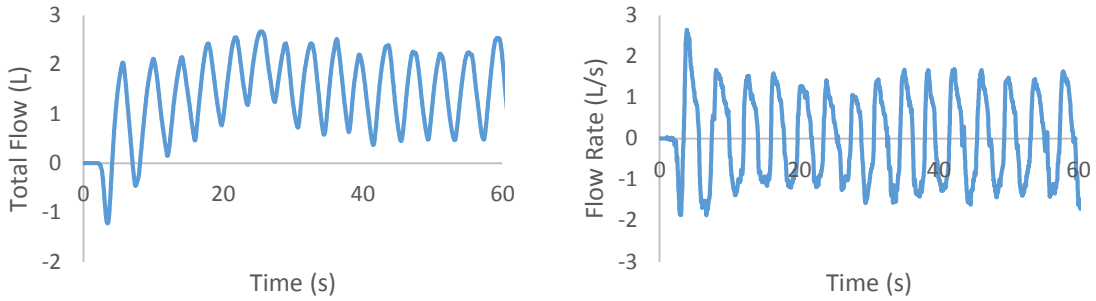

Figure C.16. M3 graphical representation of total flow and flow rate for Trial 1.

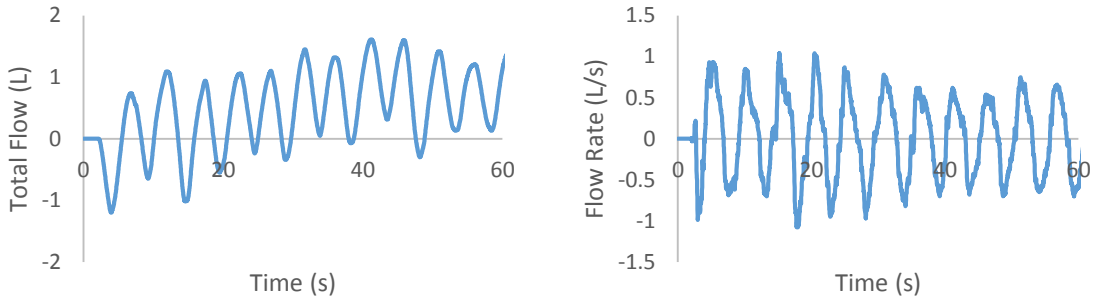

Figure C.17. M3 graphical representation of total flow and flow rate for Trial 2.

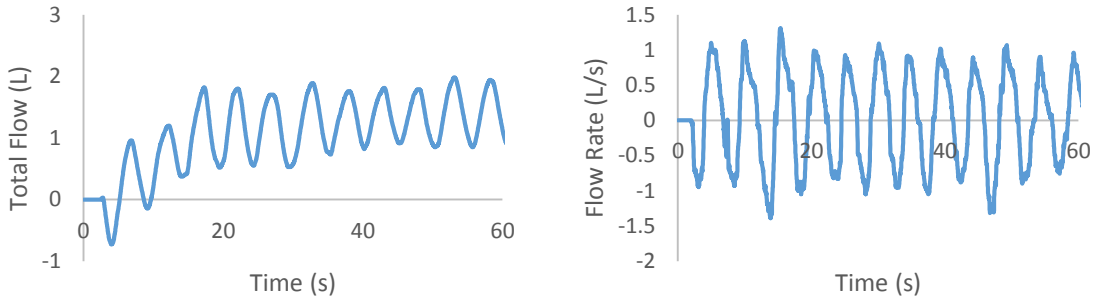

Figure C.18. M3 graphical representation of total flow and flow rate for Trial 3.

Appendix D: Statistical Analysis of Human Trials

Table D.1. ANOVA analysis of tidal volumes obtained from F1.

Anova: Single Factor

SUMMARY

Groups	*Count*	*Sum*	*Average*	*Variance*
Trial 1	9	11.55	1.2833	0.0414
Trial 2	9	4.49	0.4989	0.0048
Trial 3	11	5.15	0.4682	0.0091

ANOVA

Source of Variation	*SS*	*df*	*MS*	*F*	*P-value*	*F crit*
Between Groups	3.9903	2	1.9952	112.6106	1.56E-13	3.3690
Within Groups	0.4607	26	0.0177			
Total	4.4510	28				

Table D.2. T-Test comparison between Trial 1 and 2 of F1.

t-Test: Two-Sample Assuming Unequal Variances

	Trial 1	*Trial 2*
Mean	1.2833	0.4989
Variance	0.0414	0.0048
Observations	9	9
Hypothesized Mean Difference	0	
df	10	
t Stat	10.94146	
P(T<=t) one-tail	3.46E-07	
t Critical one-tail	1.812461	
P(T<=t) two-tail	6.93E-07	
t Critical two-tail	2.228139	

Table D.3. T-Test comparison between Trial 1 and 3 of F1.

t-Test: Two-Sample Assuming Unequal Variances

	Trial 1	*Trial 3*
Mean	1.2833	0.4682
Variance	0.0414	0.0091
Observations	9	11
Hypothesized Mean Difference	0	
df	11	
t Stat	11.06611	
P(T<=t) one-tail	1.33E-07	
t Critical one-tail	1.795885	
P(T<=t) two-tail	2.66E-07	
t Critical two-tail	2.200985	

Table D.4. T-Test comparison between Trial 2 and 3 of F1.

t-Test: Two-Sample Assuming Unequal Variances

	Trial 2	*Trial 3*
Mean	0.4989	0.4682
Variance	0.0048	0.0091
Observations	9	11
Hypothesized Mean Difference	0	
df	18	
t Stat	0.832463	
P(T<=t) one-tail	0.208028	
t Critical one-tail	1.734064	
P(T<=t) two-tail	0.416056	
t Critical two-tail	2.100922	

Table D.5. ANOVA analysis of tidal volumes obtained from F2.

Anova: Single Factor

SUMMARY

Groups	*Count*	*Sum*	*Average*	*Variance*
Trial 1	9	6.72	0.746667	0.017375
Trial 2	8	5.02	0.6275	0.002764
Trial 3	10	7.02	0.702	0.01144

ANOVA

Source of Variation	*SS*	*df*	*MS*	*F*	*P-value*	*F crit*
Between Groups	0.060964	2	0.030482	2.799621	0.080755	3.402826
Within Groups	0.26131	24	0.010888			
Total	0.322274	26				

Table D.6. ANOVA analysis of tidal volumes obtained from F3.

Anova: Single Factor

SUMMARY

Groups	*Count*	*Sum*	*Average*	*Variance*
Trial 1	11	6.03	0.548182	0.005696
Trial 2	11	6.48	0.589091	0.020469
Trial 3	9	5.04	0.56	0.015125

ANOVA

Source of Variation	*SS*	*df*	*MS*	*F*	*P-value*	*F crit*
Between Groups	0.009681	2	0.00484	0.354192	0.704839	3.340386
Within Groups	0.382655	28	0.013666			
Total	0.392335	30				

Table D.7. ANOVA analysis of tidal volumes obtained from M1.

Anova: Single Factor

SUMMARY

Groups	*Count*	*Sum*	*Average*	*Variance*
Trial 1	16	8.800432	0.550027	0.004731
Trial 2	18	11.66	0.647778	0.005218
Trial 3	17	10.48	0.616471	0.003862

ANOVA

Source of Variation	*SS*	*df*	*MS*	*F*	*P-value*	*F crit*
Between Groups	0.083385	2	0.041693	9.036377	0.000467	3.190727
Within Groups	0.221465	48	0.004614			
Total	0.30485	50				

Table D.8. T-Test comparison between Trial 1 and 2 of M1.

t-Test: Two-Sample Assuming Unequal Variances

	Trial 1	*Trial 2*
Mean	0.550027	0.647778
Variance	0.004731	0.005218
Observations	16	18
Hypothesized Mean Difference	0	
df	32	
t Stat	-4.03944	
P(T<=t) one-tail	0.000157	
t Critical one-tail	1.693889	
P(T<=t) two-tail	0.000313	
t Critical two-tail	2.036933	

Table D.9. T-Test comparison between Trial 1 and 3 of M1.

t-Test: Two-Sample Assuming Unequal Variances

	Trial 1	*Trial 3*
Mean	0.550027	0.616471
Variance	0.004731	0.003862
Observations	16	17
Hypothesized Mean Difference	0	
df	30	
t Stat	-2.90578	
P(T<=t) one-tail	0.003411	
t Critical one-tail	1.697261	
P(T<=t) two-tail	0.006821	
t Critical two-tail	2.042272	

Table D.10. T-Test comparison between Trial 2 and 3 of M1.

t-Test: Two-Sample Assuming Unequal Variances

	Trial 2	*Trial 3*
Mean	0.647778	0.616471
Variance	0.005218	0.003862
Observations	18	17
Hypothesized Mean Difference	0	
df	33	
t Stat	1.376798	
P(T<=t) one-tail	0.088922	
t Critical one-tail	1.69236	
P(T<=t) two-tail	0.177844	
t Critical two-tail	2.034515	

Table D.11. ANOVA analysis of tidal volumes obtained from M2.

Anova: Single Factor

SUMMARY

Groups	*Count*	*Sum*	*Average*	*Variance*
Trial 1	11	6.39	0.580909	0.008789
Trial 2	9	6.05	0.672222	0.009194
Trial 3	10	5.84	0.584	0.006916

ANOVA

Source of Variation	*SS*	*df*	*MS*	*F*	*P-value*	*F crit*
Between Groups	0.0509	2	0.02545	3.071946	0.062801	3.354131
Within Groups	0.223686	27	0.008285			
Total	0.274587	29				

Table D.12. ANOVA analysis of tidal volumes obtained from M3.

Anova: Single Factor

SUMMARY

Groups	*Count*	*Sum*	*Average*	*Variance*
Trial 1	14	25.59	1.827857	0.073434
Trial 2	11	21.41	1.946364	0.071245
Trial 3	11	16.24	1.476364	0.084605

ANOVA

Source of Variation	*SS*	*df*	*MS*	*F*	*P-value*	*F crit*
Between Groups	1.331055	2	0.665528	8.739015	0.0009	3.284918
Within Groups	2.513145	33	0.076156			
Total	3.8442	35				

Table D.13. T-Test comparison between Trial 1 and 2 of M3.

t-Test: Two-Sample Assuming Unequal Variances

	Trial 1	*Trial 2*
Mean	1.827857	1.946364
Variance	0.073434	0.071245
Observations	14	11
Hypothesized Mean Difference	0	
df	22	
t Stat	-1.09456	
P(T<=t) one-tail	0.142775	
t Critical one-tail	1.717144	
P(T<=t) two-tail	0.285549	
t Critical two-tail	2.073873	

Table D.14. T-Test comparison between Trial 1 and 3 of M3.

t-Test: Two-Sample Assuming Unequal Variances

	Trial 1	*Trial 3*
Mean	1.827857	1.476364
Variance	0.073434	0.084605
Observations	14	11
Hypothesized Mean Difference	0	
df	21	
t Stat	3.09034	
P(T<=t) one-tail	0.002773	
t Critical one-tail	1.720743	
P(T<=t) two-tail	0.005545	
t Critical two-tail	2.079614	

Table D.15. T-Test comparison between Trial 2 and 3 of M3.

t-Test: Two-Sample Assuming Unequal Variances

	Trial 2	*Trial 3*
Mean	1.946364	1.476364
Variance	0.071245	0.084605
Observations	11	11
Hypothesized Mean Difference	0	
df	20	
t Stat	3.948567	
P(T<=t) one-tail	0.000397	
t Critical one-tail	1.724718	
P(T<=t) two-tail	0.000793	
t Critical two-tail	2.085963	

Appendix E: Figures Pertaining to Unrestricted Porcine Lung Ventilation Trials

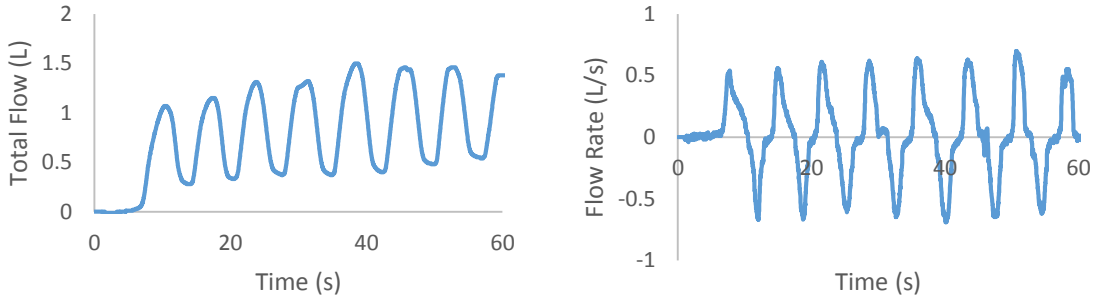

Figure E.1. Graphical representation of total flow and flow rate for Trial 1 of lung taken from 200-300 lb pig.

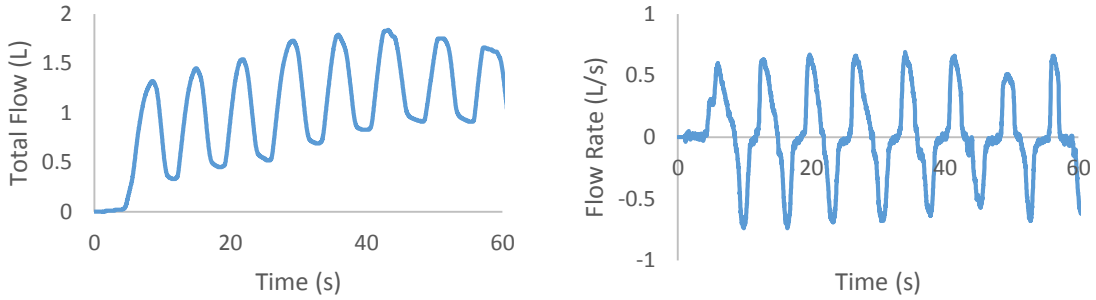

Figure E.2. Graphical representation of total flow and flow rate for Trial 2 of lung taken from 200-300 lb pig.

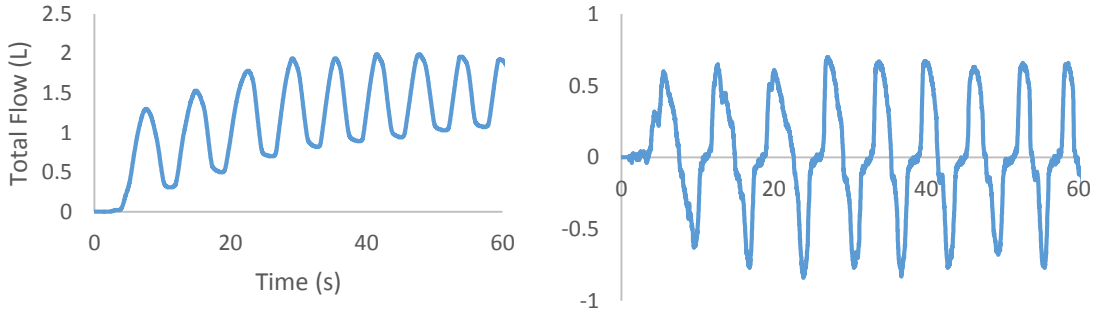

Figure E.3. Graphical representation of total flow and flow rate for Trial 3 of lung taken from 200-300 lb pig.

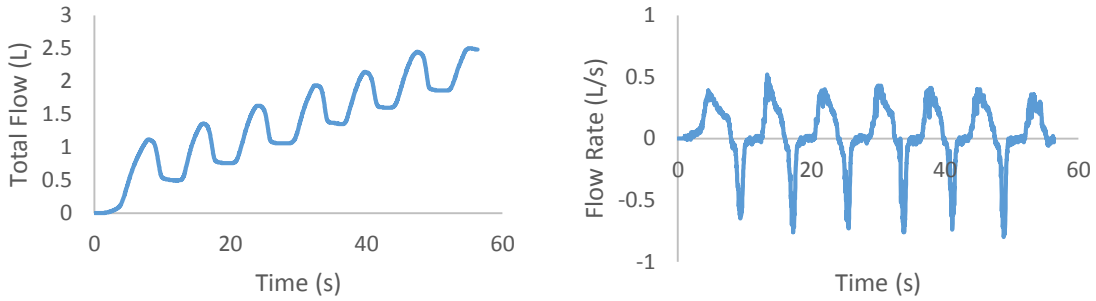

Figure E.4. Graphical representation of total flow and flow rate for Trial 1 of lung taken from 170 lb pig.

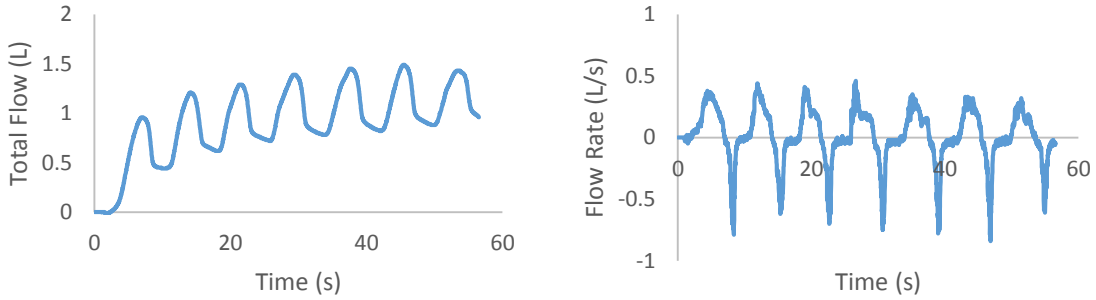

Figure E.5. Graphical representation of total flow and flow rate for Trial 2 of lung taken from 170 lb pig.

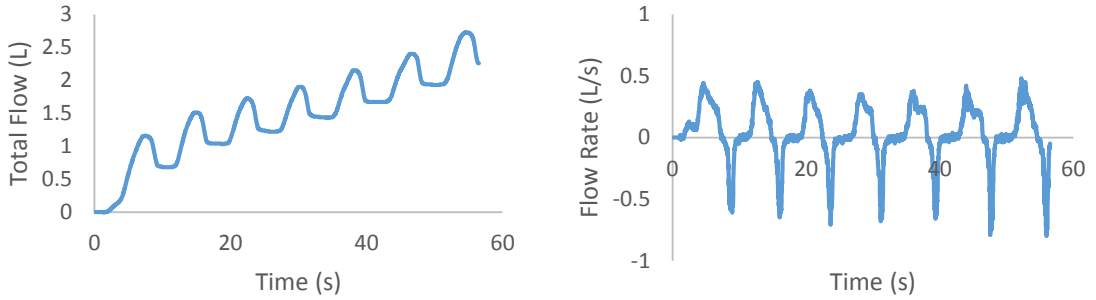

Figure E.6. Graphical representation of total flow and flow rate for Trial 3 of lung taken from 170 lb pig.

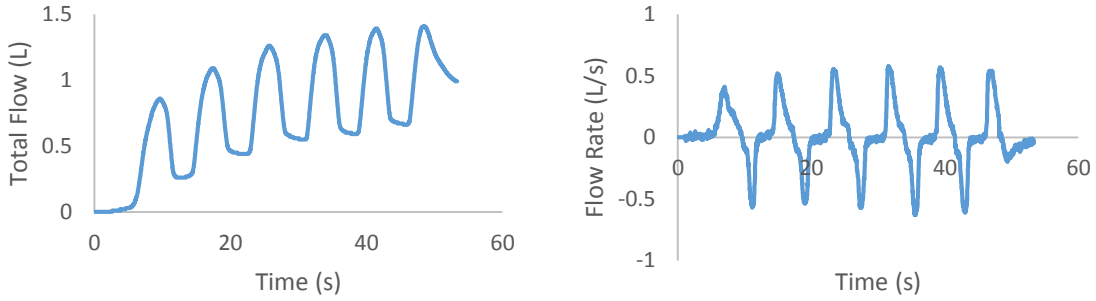

Figure E.7. Graphical representation of total flow and flow rate for Trial 1 of lung taken from 170 lb pig with 3D printed open stent in place.

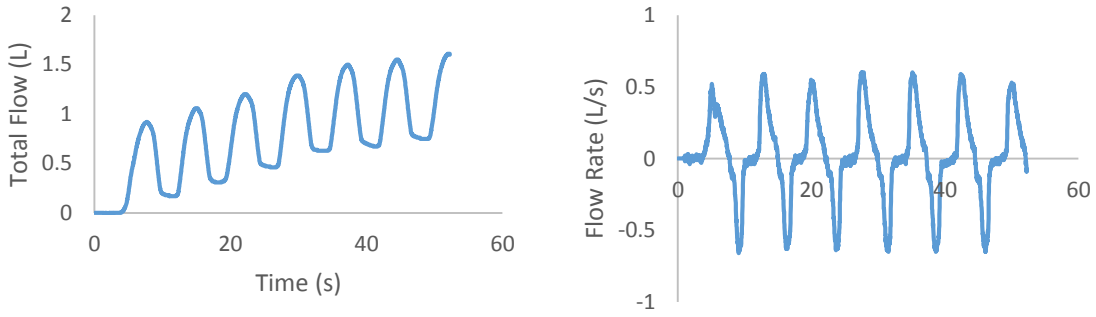

Figure E.8. Graphical representation of total flow and flow rate for Trial 2 of lung taken from 170 lb pig with 3D printed open stent in place.

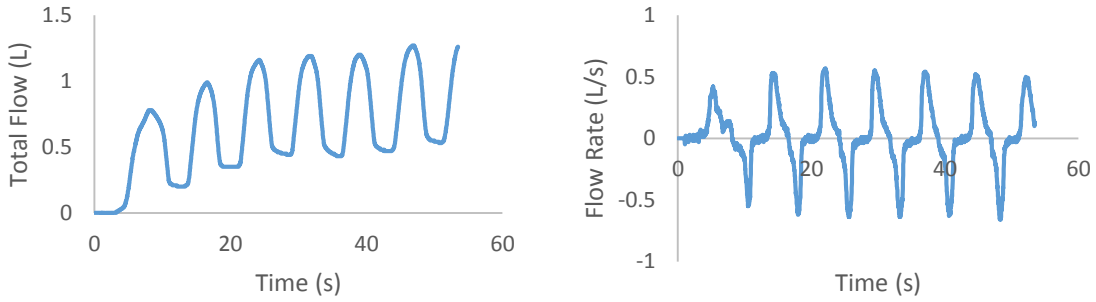

Figure E.9. Graphical representation of total flow and flow rate for Trial 3 of lung taken from 170 lb pig with 3D printed open stent in place.

Appendix F: Statistical Analysis of Unrestricted Porcine Lung Trials

Table F.1. ANOVA analysis of tidal volumes obtained from lung taken from 200-300 lb pig.

Anova: Single Factor

SUMMARY

Groups	*Count*	*Sum*	*Average*	*Variance*
Trial 1	9	8.77	0.974444	0.031253
Trial 4	10	9.59	0.959	0.008499
Trial 5	10	10.13	1.013	0.007601

ANOVA

Source of Variation	*SS*	*df*	*MS*	*F*	*P-value*	*F crit*
Between Groups	0.015409	2	0.007704	0.507225	0.608	3.369016
Within Groups	0.394922	26	0.015189			
Total	0.410331	28				

Table F.2. ANOVA analysis of tidal volumes obtained from lung taken from 170 lb pig.

Anova: Single Factor

SUMMARY

Groups	*Count*	*Sum*	*Average*	*Variance*
Trial 1	6	3.52	0.586667	0.000907
Trial 2	7	4.01	0.572857	0.00179
Trial 3	7	3.31	0.472857	0.000724

ANOVA

Source of Variation	*SS*	*df*	*MS*	*F*	*P-value*	*F crit*
Between Groups	0.052101	2	0.02605	22.57286	1.64E-05	3.591531
Within Groups	0.019619	17	0.001154			
Total	0.07172	19				

Table F.3. T-Test comparison between Trial 1 and 2 of lung taken from 170 lb pig.

t-Test: Two-Sample Assuming Unequal Variances

	Trial 1	*Trial 2*
Mean	0.586667	0.572857
Variance	0.000907	0.00179
Observations	6	7
Hypothesized Mean Difference	0	
df	11	
t Stat	0.684602	
P(T<=t) one-tail	0.253881	
t Critical one-tail	1.795885	
P(T<=t) two-tail	0.507763	
t Critical two-tail	2.200985	

Table F.4. T-Test comparison between Trial 1 and 3 of lung taken from 170 lb pig.

t-Test: Two-Sample Assuming Unequal Variances

	Trial 1	*Trial 3*
Mean	0.586667	0.472857
Variance	0.000907	0.000724
Observations	6	7
Hypothesized Mean Difference	0	
df	10	
t Stat	7.133852	
P(T<=t) one-tail	1.58E-05	
t Critical one-tail	1.812461	
P(T<=t) two-tail	3.17E-05	
t Critical two-tail	2.228139	

Table F.5. T-Test comparison between Trial 2 and 3 of lung taken from 170 lb pig.

t-Test: Two-Sample Assuming Unequal Variances

	Trial 2	*Trial 3*
Mean	0.572857	0.472857
Variance	0.00179	0.000724
Observations	7	7
Hypothesized Mean Difference	0	
df	10	
t Stat	5.276449	
P(T<=t) one-tail	0.00018	
t Critical one-tail	1.812461	
P(T<=t) two-tail	0.000359	
t Critical two-tail	2.228139	

Table F.6. ANOVA analysis of tidal volumes obtained from lung taken from 170 lb pig with open 3D printed stent in place.

Anova: Single Factor

SUMMARY

Groups	*Count*	*Sum*	*Average*	*Variance*
Trial 1	5	3.43	0.686	0.00428
Trial 2	6	4.61	0.768333	0.001097
Trial 3	6	4.17	0.695	0.00487

ANOVA

Source of Variation	*SS*	*df*	*MS*	*F*	*P-value*	*F crit*
Between Groups	0.023494	2	0.011747	3.502543	0.058429	3.738892
Within Groups	0.046953	14	0.003354			
Total	0.070447	16				

Appendix G: Figures Pertaining to Restricted Porcine Lung Ventilation Trials

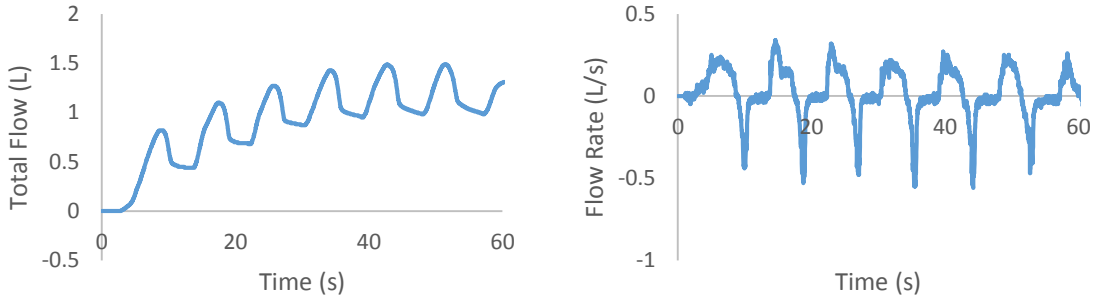

Figure G.1. Graphical representation of total flow for Trial 1 of lung taken from 170 lb pig with hose clamp causing 30% restriction to outer diameter of trachea.

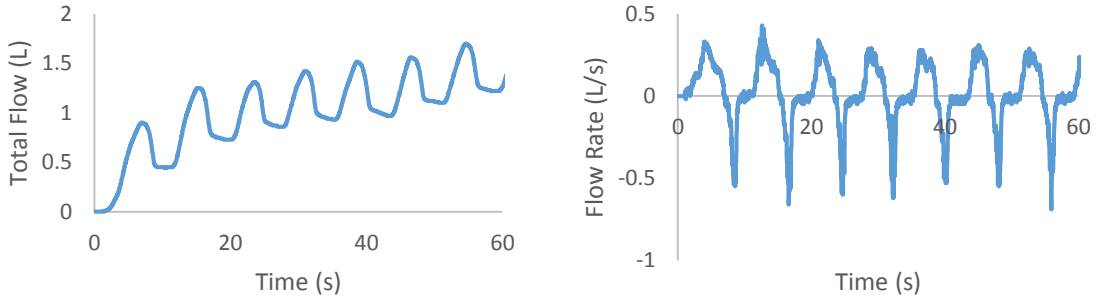

Figure G.2. Graphical representation of total flow for Trial 2 of lung taken from 170 lb pig with hose clamp causing 30% restriction to outer diameter of trachea.

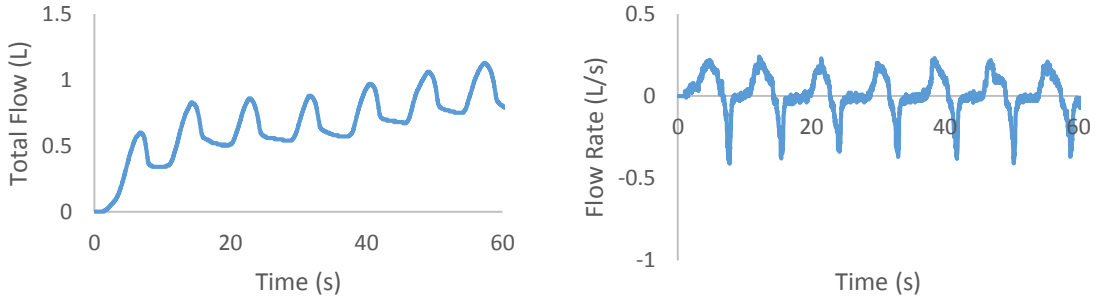

Figure G.3. Graphical representation of total flow for Trial 3 of lung taken from 170 lb pig with hose clamp causing 30% restriction to outer diameter of trachea.

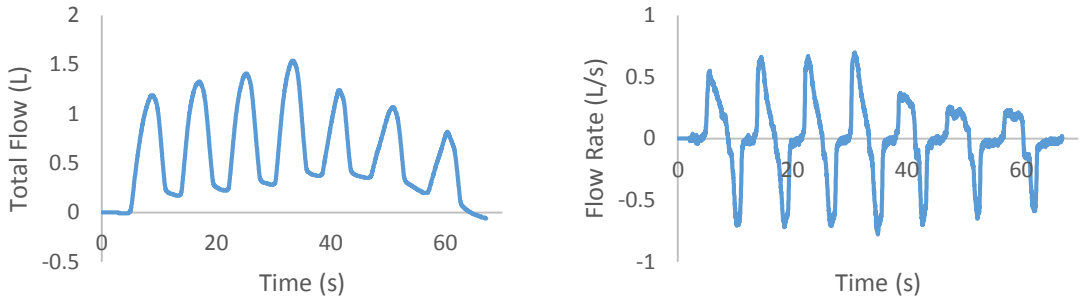

Figure G.4. Graphical representation of total flow for Trial 1 of lung taken from 170 lb pig with 3D printed stent causing 30% restriction to inner diameter of trachea.

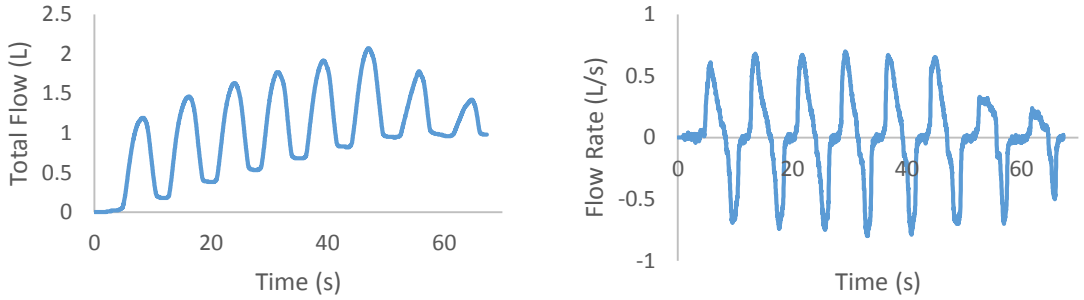

Figure G.5. Graphical representation of total flow for Trial 2 of lung taken from 170 lb pig with 3D printed stent causing 30% restriction to inner diameter of trachea.

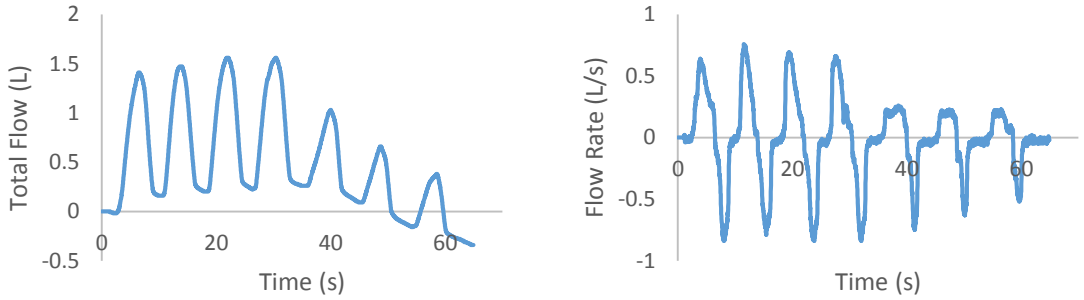

Figure G.6. Graphical representation of total flow for Trial 3 of lung taken from 170 lb pig with 3D printed stent causing 30% restriction to inner diameter of trachea.

Appendix H: Statistical Analysis of Restricted Porcine Lung Trials

Table H.1. ANOVA analysis of tidal volumes obtained from lung taken from 170 lb pig with hose clamp causing 30% restriction to outer diameter of trachea.

Anova: Single Factor

SUMMARY

Groups	*Count*	*Sum*	*Average*	*Variance*
Trial 1	6	2.7	0.45	0.00328
Trial 2	7	3.4	0.485714	0.001429
Trial 3	7	2.16	0.308571	0.000581

ANOVA

Source of Variation	*SS*	*df*	*MS*	*F*	*P-value*	*F crit*
Between Groups	0.121563	2	0.060781	36.31019	7.3E-07	3.591531
Within Groups	0.028457	17	0.001674			
Total	0.15002	19				

Table H.2. T-Test comparison between Trial 1 and 2 of lung taken from 170 lb pig with hose clamp causing 30% restriction to outer diameter of trachea.

t-Test: Two-Sample Assuming Unequal Variances

	Trial 1	*Trial 2*
Mean	0.45	0.485714
Variance	0.00328	0.001429
Observations	6	7
Hypothesized Mean Difference	0	
df	8	
t Stat	-1.30345	
P(T<=t) one-tail	0.11434	
t Critical one-tail	1.859548	
P(T<=t) two-tail	0.228679	
t Critical two-tail	2.306004	

Table H.3. T-Test comparison between Trial 1 and 3 of lung taken from 170 lb pig with hose clamp causing 30% restriction to outer diameter of trachea.

t-Test: Two-Sample Assuming Unequal Variances

	Trial 1	*Trial 3*
Mean	0.45	0.308571
Variance	0.00328	0.000581
Observations	6	7
Hypothesized Mean Difference	0	
df	7	
t Stat	5.636171	
P(T<=t) one-tail	0.000393	
t Critical one-tail	1.894579	
P(T<=t) two-tail	0.000786	
t Critical two-tail	2.364624	

Table H.4. T-Test comparison between Trial 2 and 3 of lung taken from 170 lb pig with hose clamp causing 30% restriction to outer diameter of trachea.

t-Test: Two-Sample Assuming Unequal Variances

	Trial 2	*Trial 3*
Mean	0.485714	0.308571
Variance	0.001429	0.000581
Observations	7	7
Hypothesized Mean Difference	0	
df	10	
t Stat	10.45505	
P(T<=t) one-tail	5.28E-07	
t Critical one-tail	1.812461	
P(T<=t) two-tail	1.06E-06	
t Critical two-tail	2.228139	

Table H.5. ANOVA analysis of tidal volumes obtained from lung taken from 170 lb pig with 3D printed stent causing 30% restriction to inner diameter of trachea.

Anova: Single Factor

SUMMARY

Groups	*Count*	*Sum*	*Average*	*Variance*
Trial 1	7	7.07	1.01	0.016833
Trial 2	8	7.75	0.96875	0.05567
Trial 3	7	7.62	1.088571	0.067214

ANOVA

Source of Variation	*SS*	*df*	*MS*	*F*	*P-value*	*F crit*
Between Groups	0.054627	2	0.027313	0.580503	0.569237	3.521893
Within Groups	0.893973	19	0.047051			
Total	0.9486	21				